Results in Chemistry 3 (2021) 100087

Contents lists available at ScienceDirect

Results in Chemistry

journal homepage: www.elsevier.com/locate/rechem

Biflavonoid as potential 3-chymotrypsin-like protease (3CLpro) inhibitor of SARS-Coronavirus

Yustina Hartini, Bakti Saputra, Bryan Wahono, Zerlinda Auw, Friska Indayani, Lintang Adelya, Gabriel Namba, Maywan Hariono *

Faculty of Pharmacy, Sanata Dharma University, Campus III, Paingan, Maguwoharjo, Depok, Sleman 55282, Yogyakarta, Indonesia

ARTICLE INFO

Keywords:
Biflavonoid
SARS-Coronavirus-2
3CL protease

ABSTRACT

3CL protease is one of the key proteins expressed by SARS-Coronavirus-2 cell, the potential to be targeted in the discovery of antivirus during this COVID-19 pandemic. This protein regulates the proteolysis of viral polypeptide essential in forming RNA virus. 3CL protease (3CLpro) was commonly targeted in the previous SARS-Coronavirus including bat and MERS, hence, by blocking this protein activity, the coronavirus should be eradicated. This study aims to review the potency of biflavonoid as the SARS-Coronavirus-2 3CLpro inhibitor. The review was initiated by describing the chemical structure of biflavonoid and followed by listing its natural source. Instead, the synthetic pathway of biflavonoid was also elaborated. The 3CLpro structure and its function were also illustrated followed by the list of its 3D-crystal structure available in a protein data bank. Lastly, the pharmacophores of biflavonoid have been identified as a protease inhibitor, was also discussed. This review hopefully will help researchers to obtain packed information about biflavonoid which could lead to the study in designing and discovering a novel SARS-Coronavirus-2 drug by targetting the 3CLpro enzyme.

Contents

1. Introduction . . . 1
2. Chemical structure . . . 2
3. Natural sources . . . 3
4. Synthetic sources . . . 3
5. 3-Chymotrypsine-like protease . . . 4
6. Biflavonoid as the protease –Inhibitor . . . 8
7. Perspectives . . . 10
8. Conclusion . . . 11
CRediT authorship contribution statement . . . 11
Declaration of Competing Interest . . . 11
Acknowledgement . . . 11
References . . . 11

1. Introduction

The Covid-19 pandemic has extended for almost 10 months since its outbreak in January 2020 [1]. The present statistic (by 24 October 2020) shows 43 M cases, 29 M recovered and 1.15 M death across the world. The United States of America is the country with the highest cases reported at 8.5 M approximately [2]. Meanwhile, the cases in Indonesia are still increasing. There are approximately 393,000 cases with 318,000 treated and 13,500 death [3]. This situation has made very huge impacts on all aspects of life including the economy, politics,

* Corresponding author.

https://doi.org/10.1016/j.rechem.2020.100087
Received 6 November 2020; Accepted 15 December 2020

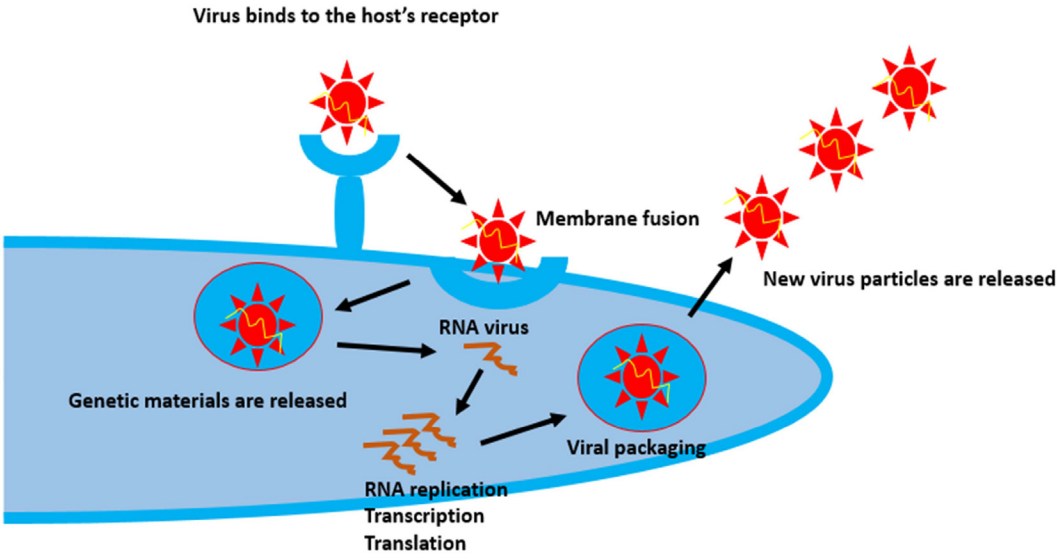

Fig. 1. The life cycle of coronaviruses is initiated by the binding of the viral cell through its protein spike (S) to the host cell's receptor namely angiotensin-converting enzyme 2 (ACE2). Upon membrane fusion (endocytosis), the virus is coated by the endosome. The following endosomal break down releases RNA from the virus into the host cell. The incoming viral genome is translated to produce two large precursor polyproteins 1a (pp1a) and 1ab (pp1ab) which are cleaved by proteases into small products. A series of subgenomic mRNA are transcripted and finally translated into viral proteins. The viral protein along with RNA is packed into virion in the ER and Golgi and then transported via vesicles and released out of the cell [9].

social, culture, health, and education. For example, United Nations Industrial Development Organization (UNIDO) reported that since April 2020, the high-income countries (30 countries) have a 18% average economic losses, whereas upper-middle-income countries (13 countries) suffer a 24% average losses. The lower-middle-income countries (6 countries) are hit by a 22% average loss, confirming the economic crisis unleashed by the pandemic, regardless of the income level [4]. The SARS-Coronavirus-2 viral vector is still a topic for debate. However, either bats or snakes are predicted as the first virus transmitting species to human [5].

Like some other coronaviruses, SARS-Coronavirus-2 is also a family of coronaviridae, which is genomically composed by the structural as well as non-structural proteins. This is an RNA virus in which on one hand, the structural protein contains S protein (spike), M protein (membrane), E protein (envelope), and N protein (nucleocapsid) [6]. On the other hand, the non-structural protein (NSP) is an open reading frame (ORF) consisting of NSP1-16 [7]. Upon entry into the host cell, the incoming viral genome is translated to produce two large precursor polyproteins 1a (pp1a) and 1ab (pp1ab) that are processed by ORF 1a-encoded viral proteinases, papain-like proteinase (PLpro), and 3C-like proteinase (3CLpro) into 16 mature non-structural proteins (NSP1–NSP16, numbered according to their order from the N-terminus to the C-terminus of the ORF 1 polyproteins). Many of the NSPs perform essential functions in viral RNA replication and transcription [8]. The virus life cycle is illustrated in Fig. 1.

One of the common studied NSPs is NSP5, in which chymotrypsin-like protease (3CLpro) is one kind of this non-structural protein [10]. 3CLpro cleaves the polyprotein into viral RNA which is then replicated and packed in the new mature virus. Therefore, by interfering with this proteolytic step, the viral RNA replication will be interrupted leading to the prevention of new viruses for further expansion. 3CLpro is one of the interesting protein targets in combating coronavirus by competitive inhibition with the peptide substrate [11].

Reviews on natural product compounds potential for SARS-Coronavirus have been published by targeting diverse proteins. These includes tanshinones, diarylheptanoids and geranylated flavonoids targeting PLpro [12], quercetine (reverse transcriptase) [13], aloeemodin and hesperitin (3CLpro) [14], apigenin (viral internal ribosome entry) [15], isatisindigotica (protease) [16], amentoflavone (biflavonoid; protease) [17], kaempferol (3a ion channel) [18], glycyrrhizin (protease) [19], tetradrine (viral S and N) [20], silvestrol (cap-dependent viral mRNA translation) [21,22], etc.

Biflavonoid is currently attractive to be proposed as the serine protease inhibitor due to the suitability of its chemical structure with the active site of the protease [23]. Serine proteases are characterized by a distinctive structure, consisting of two beta-barrel domains that converge at the catalytic active site. These enzymes can be further categorized based on their substrate specificity as either trypsin-like, chymotrypsin-like, or elastase-like. Therefore, the dimer form of biflavonoid is such a good inhibitor model that would fully occupy the two beta-barrel domain (main site and prime site) [24].

In this review, we will focus on the biflavonoid as the interesting compound, which is potential for the 3CLpro inhibitor of SARS-Coronavirus-2. The review will start by defining the chemical structure of biflavonoid and its sources from both natural products as well as synthesis. The following section would elaborate the 3CLpro structure and its function as the interesting protein target for biflavonoid. The review also summarizes the existing SARS-Coronavirus-2 3CLpro 3D crystal structure in the protein data bank. Last but not least, the current study on the biflavonoid as a diverse protease inhibitor will be carried out to give the insight mechanism on how the biflavonoid can act as a potential SARS-Coronavirus-2 antiviral agent.

2. Chemical structure

Biflavonoid is a natural product compound bearing a dimer of two sets of flavonoid, linked by either C–C or C-O bond [25,26]. The flavonoid itself is chemically constructed by a 15-C skeleton, which is divided into two aromatic rings (Ring A and Ring B) and connected by a heterocyclic ring having α, β- unsaturated carbonyl chain [27]. In addition to flavonoid being the major form of such compound class, there are two kind of analogs which enrich the flavonoid structural diversity. They are isoflavonoid (derived from 3-phenylchromen-4-one (3-phenyl-1,4-benzopyrone) and neoflavonoid (derived from 4-phenylcoumarine (4-phenyl-1,2-benzopyrone). Other sub-groups of flavonoid including flavan, flavanone, flavanonol, anthocyanidin,

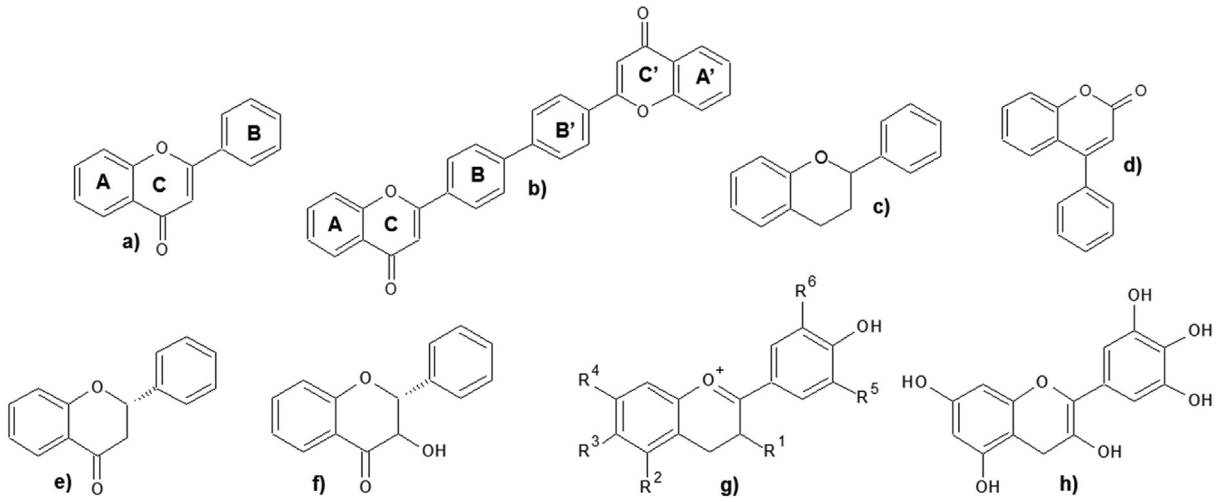

Fig. 2. The structures of a) flavonoid, b) biflavonoid, c) isoflavonoid, d) neoflavonoid, e) flavanone, f) flavanonol, g) anthocyanidin and h) anthoxantin which are naturally occurred in plants.

and anthoxantin are also widely distributed among natural resources [28]. Fig. 2 illustrates the structure of flavonoid and their analogs.

The aromatic rings are often decorated by poly-hydroxy group. Therefore, this compound's class are frequently called polyphenolic compounds. The presence of OH group has also given chance for the flavonoid to be biosynthetically formed in a glycoside. The sugar moiety in the glycosidic form makes the flavonoid more soluble in water than organic solvents due to the polar character of the sugar [29,30].

Spectroscopically, alike to the polyphenolic flavonoid, the yellowish biflavonoid absorbs UV light at 500–600 nm. The colorimetric reaction namely bathochromic shift (redshift) occurs when it reacts with an alkaline solution to prolong the maximum wavelength (650 nm). Similarly, polyvalent ion such as Al^{3+} may shift the wavelength into a hypsochromic shift (blue shift) with a lower wavelength (450 nm) [31]. Using the fourier transform infrared (FTIR) spectroscopy, the carbonyl of chromone group stretching vibration is transmitted at 1600 $cm^{-1,}$ Meanwhile, the vinyl aromatic group appears at 3600 cm^{-1} as a bending vibration [32]. The proton of biflavonoid is indicated as multiplet signals around 6–8 ppm which often overlap in *trans/ cis* configuration protons of α, β- unsaturated carbonyl chain as confirmed by nuclear magnetic resonance (NMR) spectroscopy. In conjunction, the carbon signal of the carbonyl chromone group is indicated at 160 ppm, whereas the vinylic aromatic carbon appears at 150 ppm. Using a mass spectroscopy, the origin of the flavonoid skeleton could be the most stable mass/ion (base peak) during the fragmentation due to the electron impact bombardment [33].

3. Natural sources

A naturally occurring biflavonoid is distributed in various plant species. The first isolated natural biflavonoid was from *Ochna squarrosa* Linn. (Ochnaceae) [34] and later was from *Lonicera japonica* (Caprifoliaceae) [35]. *Torreya nucifera* was also identified as the natural source producing four biflavonoids [36]. Amentoflavone is another kind of biflavonoid isolated from abroad family of plants such as selaginellaceae, cupressaceae, euphorbiaceae, podocarpaceae, and calophyllaceae [37]. It was reported that at least 127 biflavonoids are distributed among plants, but the most occurrences are *Gingko biloba*, *Lobelia chinensis*, *Polygala sibirica*, *Ranunculus ternatus*, *Selaginella pulvinata*, and *Selagenella tamariscina* [37].

A more recent study had identified the biflavonoid I3′ II8-binaringenin in drupes of *Schinus terebinthifolius*, which was indicated by UHPLC-MS [38]. Five biflavonoids were lately found in *Ceratodon purpureus* presenting a diastereomeric form in the second biflavonoid [39]. In the same year, three biflavonoid types were also discovered in *Selaginella doederleinii* including the amentoflavone type, robustaflavone type, and hinokiflavone type [40]. From the zingiberaceae family, new biflavonoids with flavanone-chalcone type can be found in fingerroot (*Boesenbergia rotunda*) [41]. The pure biflavonoid with aglycones morelloflavone (Mo) type, volkensiflavone (Vo) type, as well as the morelloflavone's glycoside fukugiside (Fu) type was characterized in *Garcinia madruno* [42]. The genus of garcinia again shows its resource of biflavonoid by the discovery of seven compounds including volkensiflavone, fukugetin, fukugeside, GB 1a, GB 1a glucoside, GB 2a, and GB 2a glucoside from *Garcinia xanthochymus* fruits [43]. Fig. 3 illustrates the chemical structure of hinokiflavone, ochnaflavone, amentoflavone, morelloflavone, and volkensiflavone. For more data, Table 1 tabulates the various studies reporting biflavonid found in a natural source in the last three years.

4. Synthetic sources

Instead of natural sources, biflavonoid is also produced via a synthetic pathway. This usually aims to derivatize the biflavonoid lead compound into a modified diverse functional group that could be responsible for its biological activity. Besides, the synthetic pathway could be more reproducible than isolating the biflavonoid from its genuine natural sources. This will proportionally reduce the cost of production as well as increase the yields [74,75].

Biflavonoid is synthetically formed by two units (monomer) of flavonoid undergoing the Ullmann coupling reaction [76]. This reaction forms a diaryl ether link between two units of flavonoid, which is conditioned by mixing them with an alkaline carbonate solution, *N*, *N*-dimethylacetamide, and dry toluene solvent under nitrogen exposure, followed by heating the mixture above 100 °C for several hours [77]. The total synthesis of biflavonoid is initiated by reacting *ortho*-hydroxy acetophenone with benzaldehyde under Claissen Smith condensation to form chalcone as the intermediate compound [78]. The next step is the synthesis of flavone (monomer) by iodinating the chalcone using DMSO as the solvent [79]. The detailed total synthesis of biflavonoid is schemed out in Scheme 1.

An interesting biflavonoid was constructed according to the naringenin monomer by reacting to the available phloroglucinol and 4-hydroxy- or 4-methoxybenzaldehyde. Naringenin is the flavanone-skeleton structure attached by three hydroxy groups at the 4′, 5, and

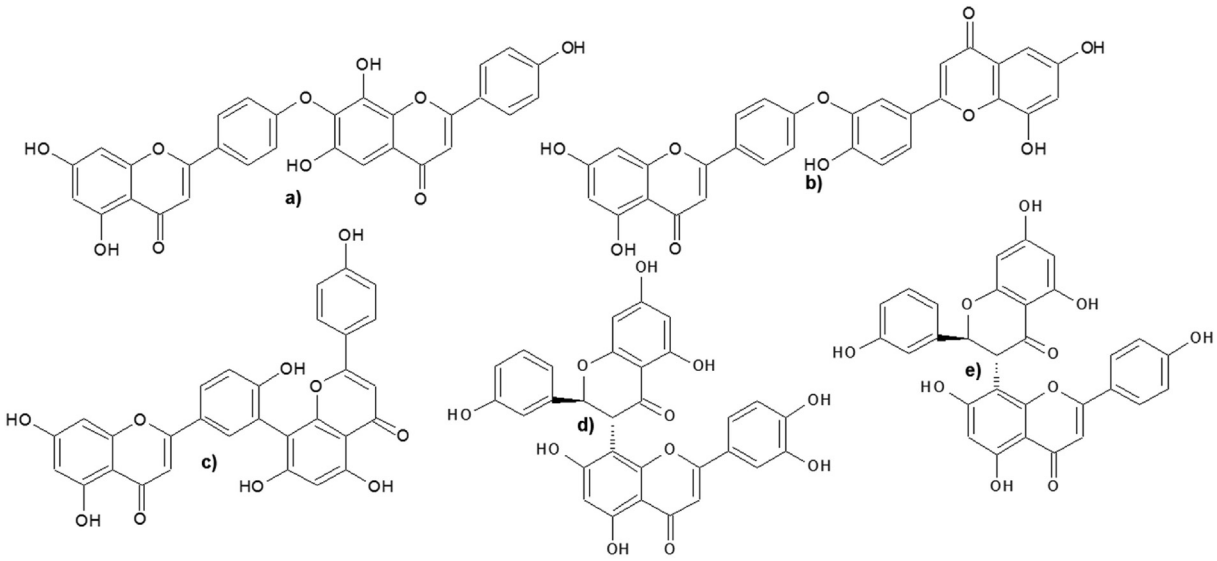

Fig. 3. The chemical structures of earlier biflavonoid found in plants: a) hinokiflavone, b) ochnaflavone, c) amentoflavone, d) morelloflavone, and e) volkensiflavone.

7 carbons. The product was confirmed as 3′,3‴-binaringenin, and four related biflavonoids with a considerably good yield (15–35%) [81].

Biflavonoid was also prepared electrochemically by reacting to flavonol isorhamnetin, $LiClO_4$, and amine in acetonitrile solvent. The mixture was electrolyzed in a diaphragm cell at anodic current density of 5 mA/cm^2 for 3.5 h. Platinum-plated with a working surface of 2 cm^2 was used as the anode. Once the electrolysis was completed, about 90% of the acetonitrile was distilled from the anode compartment. Further purification using chromatography column was applied and followed by recrystallization to obtain the biflavonoid product with a good yield (60–70%) [82].

A step-economical preparation of a very rare biflavonoid has been performed by combining the methylated biaurone undergoing a modular and divergent synthesis strategy. The divergent synthesis was carried out by using bialdehyde as the building block such as isophthalaldehyde, terephthalaldehyde, and benzene-1,3,5-tricarbaldehyde to produce the chalcone intermediate under Claissen Smith condensation. The following reaction was oxidative cyclization to obtain the biflavonoid as the targeted compound. Interestingly, instead of biflavonoid, the divergent method is also applied in the production of triflavonoid [83].

The synthesis of biflavonoid was further explored by applying the Suzuki-Miyaura cross-coupling reaction followed by alcohol methylation for the synthesis of rare 'hybrid' derivatives. These derivatives belong to different sub-classes of monomers. The second biflavonoid was constructed as homodimeric compounds in which a methylenedioxy group acts as the linker between the two flavonoid monomers. This reaction facilitates the probing of uncharted regions of biologically interesting chemical space [84].

The first stereodivergent synthesis of biflavanone was conducted by exclusively controlling the temperature to produce a stereoselective product. The scaffold of 2,2′-biflavanones was attached by diverse substitution at the phenyl ring and conditioned by SmI_2/Methanol/THF, confirmed by a highly selected good yield for both stereoisomers of the expected compounds. On one hand, the (R*,R*)-stereoisomer was only formed when the temperature was controlled at −40 °C. On the other hand, the reaction generated the (R*,S*)-isomer when the mixture was refluxed [85]. The control of regioselective reaction was performed using aromatic prenyltransferase from *Aspergillus terreus* (AtaPT). Prenylation was applied to produce biflavonoids 1–3 dimerized connected by a diphenyl linkage at the hydrogen bond involving C5″–OH group. This OH is chemically less accessible than other OH groups in the ring. The AtaPT was used as the substrate that successfully yielded the different regio and chemoselective products. This study would be recommended for developing green synthetic reactions for such prenylated biflavonoids [86].

5. 3-Chymotrypsine-like protease

The extensive process of proteolysis releases the functional polypeptides which are mainly achieved by the main proteinase and are also frequently named 3C-like proteinase (3CLpro). This indicates a similar cleavage site with the early picornavirus of 3C proteinases (3Cpro), although further studies showed that the similarity is limited by two families of the protease. 3CLpro cleaves at least 11 conserved amino acid residues includes GLN---(SER, ALA, GLY) sequences (the cleavage site is indicated by ---) [87]. This process is initiated by the autocleavage of its enzyme from two polypeptides (polypeptide A and polypeptide B). There are three non-canonical 3CLpro cleavage sites at the P2 position employing PHE, MET, or VAL residues in SARS-Coronavirus polyproteins. The cleavage site of 3CLpro SARS-Coronavirus is illustrated in Fig. 4 [10,88].

The availability of experimentally determined three-dimensional (3D) structures of the SARS-Coronavirus-2 3CLpro has greatly aided in the design of anti-SARS-Coronavirus-2 drug [91]. Recently, the sudden increase in the number of crystal structures of 3CLpro is deposited in the protein data bank (PDB) [92]. Most of the earlier crystal structures are devoid of inhibitor. Thus, it could not explain the particular binding site of 3CLpro properly [93]. Therefore, many efforts conducted to understand the structure and function of 3CLpro relied mainly on the models developed based on the crystal structures of other betacoronavirus such as SARS-Coronavirus, MERS, Bat Corona, etc [94].

To date, there are more than 100 3D structures of SARS-Coronavirus-2 3CLpro deposited in the protein data bank (PDB) (www.rcsb.org). In general, the crystal structures of 3CLpro reveal the presence of three structural domains in each monomer, in which domains I (position 8–101), II (position 102–184), and III (position 201–303) have a chymotrypsin-like characteristic fold with a catalytic cysteine (CYS145) and histidine (HIS41). This is linked to a third C-terminal domain by a long loop (position 185–200) by orienting the

Table 1
Biflavonoids from natural resources have been reported in the last three years.

No	Biflavonoid	Plants	References
1	dihydrodaphnodorin B	*Fumana procumbens*	[44]
2	daphnodorin B	*Fumana procumbens*	[44]
3	volkesiflavone	*Garcinia gardneriana*	[45]
4	morelloflavone	*Garcinia gardneriana, Garcinia madruno*	[45]
5	7,7″-di-*O*-methylchamaejasmin	*Ormocarpum kirkii*	[46]
6	campylospermone A	*Ormocarpum kirkii*	[46]
7	a dimeric chromene [diphysin	*Ormocarpum kirkii*	[46]
8	amentoflavone 7′′-*O*-*β*-*d*-glucopyranoside	*Ginkgo Biloba*	[47]
9	bilobetin	*Ginkgo Biloba*	[47]
10	isoginkgetin	*Ginkgo Biloba*	[47]
11	sciadopitysin	*Ginkgo Biloba*	[48]
12	agathisflavone	*Schinus terebinthifolius; Anacardium occidentale*	[49,50]
13	tetrahydroamentoflavone	*Schinus terebinthifolius*	[49]
14	uncinatabiflavone C 7-methyl ether	*Selaginella uncinata*	[50]
15	7, 4′, 7′″, 4′″-tetra-*O*-methyl amentoflavone	*Cephalotaxus harringtonia*	[51]
16	7, 4′, 7″-tri-*O*-methyl amentoflavone	*Cephalotaxus harringtonia*	[51]
17	sequoiaflavone	*Cephalotaxus harringtonia; Ouratea ferruginea*	[51,52]
18	amentoflavone monomethoxy derivatives	*Cunninghamia lanceolata*	[53]
19	dihydrochalcone flavanone	*Sophora flavescens*	[54]
20	2′,3′-dihydroochnaflavone	*Ochna mauritiana*	[55]
21	dulcisbiflavonoid B	*Garcinia dulcis*	[56]
22	dulcisbiflavonoid C	*Garcinia dulcis*	[56]
23	umcephabiflovin A	*Cephalotaxus oliveri*	[57]
24	umcephabiflovin B	*Cephalotaxus oliveri*	[57]
25	S-taiwanhomoflavone-B	*Cephalotaxus oliveri*	[57]
26	5, 6, 6′-trihydroxy-[1,1′-biphenyl]-3,3′-dicarboxylic acid	*Mesua ferrea*	[58]
27	fukugiside	*Garcinia madruno*	[59]
28	neochamaejasmin B	*Stellera chamaejasme*	[60]
29	oliveriflavone A, B, and C	*Cephalotaxus oliveri*	[61]
30	rhusflavanone	*Mesua ferrea*	[62]
31	mesuaferrone B	*Mesua ferrea*	[62]
35	sinodiflavonoids A	*Sinopodophyllum emodi*	[63]
36	sinodiflavonoids B	*Sinopodophyllum emodi*	[63]
37	oxytrodiflavanone A	*Oxytropis chiliophylla*	[64]
38	oxytrochalcoflavanones A	*Oxytropis chiliophylla*	[64]
39	oxytrochalcoflavanones B	*Oxytropis chiliophylla*	[64]
40	hinokiflavone	*Selaginella sinensis*	[65]
41	isocampylospermone A	*Ochna Serrulata*	[66]
42	campylospermone A	*Ochna Serrulata*	[66]
43	cupressuflavone	*Cupressus sempervirens*	[67]
44	(8-hydroxy-3′-*β*-*D*-galactosyl-isoflavone)-2′-8′′-(4′′′-hydroxy-flavone)-biflavone	*Solanum nigrum*	[68]
45	2′,3′,5-trihydroxy-5′′-methoxy-3′′-*O*- α-glucosyl-3–4′′“-*O*-biflavone	*Solanum nigrum*	[68]
46	7′-*O*-methyl hinokiflavone	*Selaginella tamariscina*	[69]
47	(2*R*,3*S*)-volkensiflavone-7-*O*-*β*-acetylglucopyranoside	*Allanblackia floribunda*	[70]
48	(2*S*,3*S*)-morelloflavone-7-*O*-β-acetylglucopyranoside	*Allanblackia floribunda*	[70]
49	(*S*)-2″*R*,3″*R*- and (*R*)-2″*S*,3″*S*-dihydro-3″-hydroxyamentoflavone-7- methyl ether	*Cardiocrinum giganteum*	[71]
50	(*S*)-2″*R*,3″*R*- and (*R*)-2″*S*,3″*S*-dihydro-3″-hydroxyamentoflavone	*Cardiocrinum giganteum*	[71]
51	4,4′,7-tri-*O*-methylisocampylospermone A	*Ochna serrulata*	[72]
52	4′′′-de-*O*-methylafzelone A	*Ochna serrulata*	[72]
53	serrulone A	*Ochna serrulata*	[72]
54	sumaflavone	*Juniperus phoenicea*	[73]

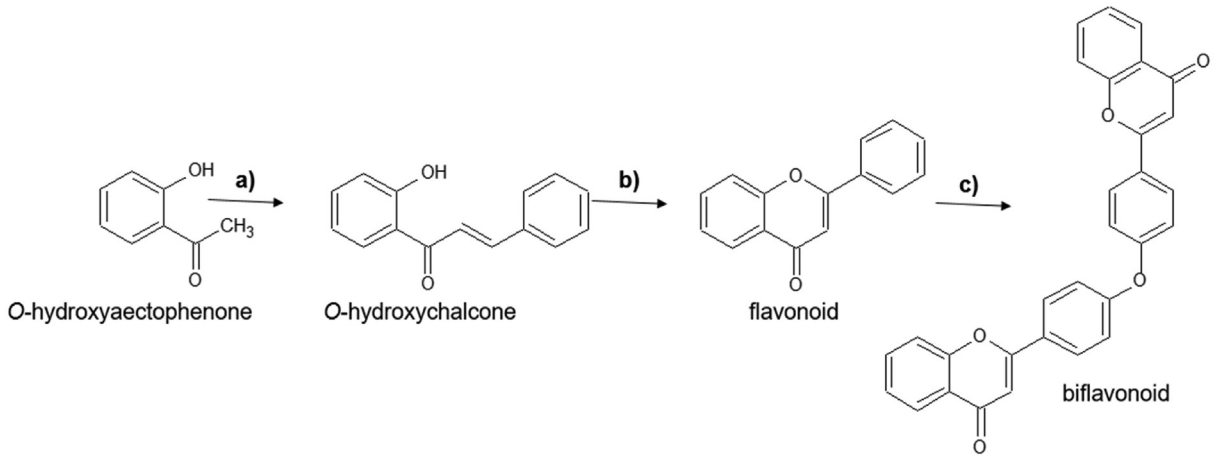

Scheme 1. Total synthesis of biflavonoid. Reagents and conditions: a) benzaldehyde, KOH, MeOH, rt, overnight, 70–87%; b) I_2, DMSO, 100 °C, overnight, 75–86%; and c) Ullmann modified coupling reaction, 8–58% [80].

3CLpro Cleavage Site	P6	P5	P4	P3	P2	P1	P1′	P2′	P3′	P4′	P5′	Relative Kcal/Km
nsp4/5	T	S	A	V	L	Q	S	G	F	R	K	100%
nsp5/6	S	G	V	T	F	Q	G	K	F	K	K	41%
nsp6/7	K	V	A	T	V	Q	S	K	M	S	D	3%
nsp7/8	N	R	A	T	L	Q	A	I	A	S	E	5%
nsp8/9	S	A	V	K	L	Q	N	N	E	L	S	2%
nsp9/10	A	T	V	R	L	Q	A	G	N	A	T	22%
nsp10-12	R	E	P	L	M	Q	S	A	D	A	S	0,2%
nsp12/13	P	H	T	V	L	Q	A	V	G	A	C	8%
nsp13/14	N	V	A	T	L	Q	A	E	N	V	T	9%
nsp14/15	T	F	T	R	L	Q	S	L	E	N	V	28%
nsp16/15	F	Y	P	K	L	Q	A	S	Q	A	W	27%

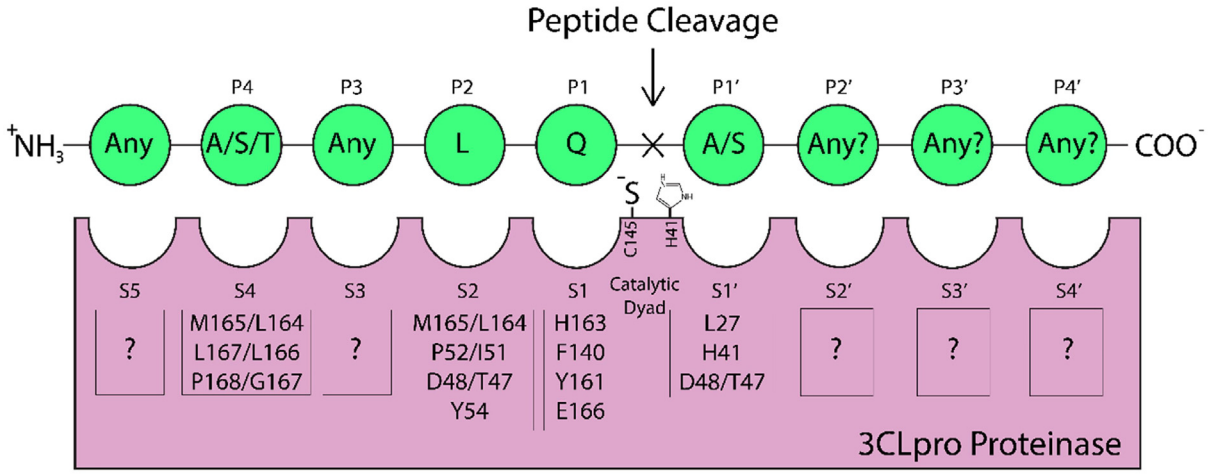

Fig. 4. The 3CLpro cleavage sites of SARS Coronavirus which recognize 11 sequences of peptide substrate with their respective Kcal/Km. These Kcal/Km values reflect the canonical recognition which is supported by the recognition sites of a series of other coronavirus 3C proteases [89,90].

N-terminal residues that are essential for the dimerization [95-98]. Domain I and domain II are decorated in an antiparallel β-barrel structure, whereas domain III is composed of five α-helices arranged in a globular cluster. The helical domains of the two monomers form a dimer through H-bond interactions from the end to end of the N-terminal residues and the key residues from the individual monomers. The catalytic activity is suggested to be contributed by the salt bridge between the N-terminal SER1 of one monomer and GLU166 of the other monomer [97,99]. Table 2 presents the 115 3D-structures of 3CLpro available in the protein data bank.

SARS-Coronavirus-2 3CL pro in complex with a novel inhibitor 5,6,7-trihydroxy-2-phenyl-4H-chromen-4-one solved its 3D-crystal structure in 2.20 Å solution. This flavonoid inhibitor binds the active site of the protease through the hydrogen bond interaction between *ortho*-hydroxyphenyl (ring A) of the ligand with GLY143, and the carbonyl group of ring C with GLU166. The non-bonding interaction was also observed between the phenyl of ring B with HIS41 and CYS44. Fig. 5 illustrates the interaction between 5,6,7-trihydroxy-2-phenyl-4 H-chromen-4-one and the active site of SARS-Coronavirus-2 3CLpro (PDB ID 6M2N) [100].

Two peptidomimetic-based inhibitors are complexed with SARS-Coronavirus-2 in different monomer of trimer with 2.15 Å of the crystal resolution (PDB 6WTT) [101]. (1*S*,2*S*)-2-({*N*-[(benzyloxy) carbonyl]-*L*-leucyl}amino)-1-hydroxy-3-[(3*S*)-2-oxopyrrolidin-3-yl]propane-1-sulfonic acid binds the active site in monomer A by interacting it with CYS145, GLU166, GLN189, HIS164, and PHE140 at the respective atoms of O (OH), O (C = O), H (NH-amide), H (NH-amide) and H (NH-pyrrolidinone) (Fig. 6). Monomer B demonstrates the same binding mode as monomer A, whereas monomer C is bound by *N* ~ 2 ~ -[(benzyloxy)carbonyl]-*N*-[(1*R*,2*S*)-1-hydroxy-3-[(3S)-2-oxopyrrolidin-3-yl]-1-(trimethyl-lambda ~ 4 ~ -sulfanyl)propan-2-yl]-*L*-leucinamide. In monomer C, the ligand interacts with GLU166, HIS164, HIS41, and GLN189 at the respective atoms of O (C = O), N (NH-amide) and N- (NH-pyrrolidinone), O (OH), and N (NH-amide).

A class of imidazole-4-carboxamide compound was also complexed to SARS-Coronavirus-2 3CLpro and the 3D crystal structure was resolved at 1.46 Å (PDB ID 6W79; Fig. 7a) [102]. This inhibitor binds the active site of the protease by interacting it with the residues GLY143 and GLU166 at atom O (C=O-amide) and also the next O (C=O-amide), respectively. The hydrophobic interaction was also performed via the interaction between ASN142- O (C=O-amide), THR26-H-CH-imidazole), CYS145-imidazole ring, and LEU141-ASN142-pyridine.

An inhibitor which was a repurposed drug from antineoplastic, was complexed with SARS-Coronavirus-2 3CLpro in 1.60 Å of 3D-crystal resolution (PDB ID 7BUY; Fig. 7b) [103]. Interestingly, this inhibitor binds covalently (distance 1.8 Å) at its O (C=O) to CYS145 which is one of the catalytic site residues. This inhibitor's name is carmofur,

Table 2
The list of 3CLpro 3D-crystal structure available in protein data bank.

PDB ID	Co-crystallized Ligand	Resolution (Å)	Reference
6M2N	5,6,7-trihydroxy-2-phenyl-4H-chromen-4-one	2.20	[100]
6M2Q	–	1.70	[100]
6WQF	–	2.30	[105]
6XB1	1-ethyl-pyrrolidine-2,5-dione	1.80	[106]
6XB0	dimethyl sulfoxide	1.80	[106]
6XB2	1-ethyl-pyrrolidine-2,5-dione, dimethyl sulfoxide	2.10	[106]
6L00 and 6LNY	(2~{*S*})-4-methyl-~{*N*}-[(2~{*S*})-1-oxidanylidene-3-[(3~{*S*})-2-oxidanylidenepyrrolidin-3-yl]propan-2-yl]-2-[[(~{*E*})-3-phenylprop-2-enoyl]amino]pentanamide	1.94 and 2.25	[107]
7JFQ	1,2-ethanediol, formic acid	1.55	[108]
6XKF	1,2-ethanediol, chloride ion	1.80	[109]
6XKH	1,2-ethanediol, acetate ion, formic acid	1.28	[110]
6XOA	1,2-ethanediol	2.10	[111]
6LNQ	*N*-[(2*S*)-3-methyl-1-[[(2*S*)-4-methyl-1-oxidanylidene-1-[[(2*S*)-1-oxidanylidene-3-[(3*S*)-2-oxidanylidenepyrrolidin-3-yl]propan-2-yl]amino]pentan-2-yl]amino]-1-oxidanylidene-butan-2-yl]-1H-indole-2-carboxamide	2.24	[107]
7JUN	–	2.30	[112]
7JR3	–	1.55	[113]
7JR4	–	1.55	[114]
6XHU	–	1.80	[115]
6XQT	(1*R*,2*S*,5*S*)-3-[*N*-({1-[(*tert*-butylsulfonyl)methyl]cyclohexyl}carbamoyl)-3-methyl-*L*-valyl]-*N*-{(1*S*)-1-[(1*R*)-2-(cyclopropylamino)-1-hydroxy-2-oxoethyl]pentyl}-6,6-dimethyl-3-azabicyclo[3.1.0]hexane-2-carboxamide	2.30	[116]
6XQS	(1*S*,3a*R*,6a*S*)-2-[(2*S*)-2-({(2*S*)-2-cyclohexyl-2-[(pyrazin-2-ylcarbonyl)amino]acetyl}amino)-3,3-dimethylbutanoyl]-*N*-[(2*R*,3*S*)-1-(cyclopropylamino)-2-hydroxy-1-oxohexan-3-yl]octahydrocyclopenta[c]pyrrole-1-carboxamide	1.90	[116]
6XQU	boceprevir (bound form)	2.20	[116]
6W2A	[4,4-*bis*(fluoranyl)cyclohexyl]methyl ~{*N*}-[(2~{*S*})-1-[[(1~{*R*},2~{*S*})-1-[*bis*(oxidanyl)-oxidanylidene-$l^{5}-sulfanyl]-1-oxidanyl-3-[(3~{*S*})-2-oxidanylidenepyrrolidin-3-yl]propan-2-yl]amino]-4-methyl-1-oxidanylidene-pentan-2-yl]carbamate, (1*S*,2*S*)-2-[(*N*-{[(4,4-difluorocyclohexyl)methoxy]carbonyl}-*L*-leucyl)amino]-1-hydroxy-3-[(3*S*)-2-oxopyrrolidin-3-yl]propane-1-sulfonic acid	1.65	[117]
6WTK	*N* ~ 2 ~ -[(benzyloxy)carbonyl]-*N*-{(2*S*)-1-hydroxy-3-[(3*S*)-2-oxopyrrolidin-3-yl]propan-2-yl}-*L*-leucinamide	2.00	[118]
6WTM	–	1.85	[118]
6WTJ	(1*S*,2*S*)-2-({*N*-[(benzyloxy)carbonyl]-*L*-leucyl}amino)-1-hydroxy-3-[(3*S*)-2-oxopyrrolidin-3-yl]propane-1-sulfonic acid	1.90	[118]
6 W63 and 6 W79	*N*-(4-*tert*-butylphenyl)-*N*-[(1R)-2-(cyclohexylamino)-2-oxo-1-(pyridin-3-yl)ethyl]-1H-imidazole-4-carboxamide	2.10	[102]
6WCO	N-(4-*tert*-butylphenyl)-N-[(1R)-2-(cyclopentylamino)-2-oxo-1-(pyridin-3-yl)ethyl]-1H-imidazole-4-carboxamide	1.48	[102]
6XBH	–	1.60	[119]
6XBG	–	1.45	[120]
6XFN	–	1.70	[121]
7JU7	Masitinib	1.60	[122]
3SZN	ethyl (4*R*)-4-({*N*-[(benzyloxy)carbonyl]-l-phenylalanyl}amino)-5-[(3*S*)-2-oxopyrrolidin-3-yl]pentanoate	1.69	[123]
3SNE	2-(*N*-morpholino)-ethanesulfonic acid	2.60	[124]
3SNA, 3SNB, and 3SNC	–	3.05, 2.40 and 2.58	[124]
6XBI	–	1.70	[125]
6XHO	ethyl (2*E*,4*S*)-4-{[*N*-(4-methoxy-1H-indole-2-carbonyl)-*L*-leucyl]amino}-5-[(3S)-2-oxopyrrolidin-3-yl]pent-2-enoate	1.45	[126]
6XHN	(3S)-3-{[*N*-(4-methoxy-1H-indole-2-carbonyl)-*L*-leucyl]amino}-2-oxo-4-[(3*S*)-2-oxopyrrolidin-3-yl]butyl 2-cyanobenzoate	1.38	[126]
6XHL and 6XHM	*N*-[(2*S*)-1-({(2*S*)-4-hydroxy-3-oxo-1-[(3*S*)-2-oxopyrrolidin-3-yl]butan-2-yl}amino)-4-methyl-1-oxopentan-2-yl]-4-methoxy-1H-indole-2-carboxamide	1.47 and 1.41	[126]
6XA4	–	1.65	[127]
6Y2E	–	1.75	[128]
6Y2G, 6Y2F	~{*tert*}-butyl~{*N*}-[1-[(2~{*S*})-3-cyclopropyl-1-oxidanylidene-1-[[(2~{*S*},3~{*R*})-3-oxidanyl-4-oxidanylidene-1-[(3~{*S*})-2-oxidanylidenepyrrolidin-3-yl]-4-[(phenylmethyl)amino]butan-2-yl]amino]propan-2-yl]-2-oxidanylidene-pyridin-3-yl]carbamate	2.20, and 1.95	[128]
7JKV	*N*-[(2*S*)-1-({(1*S*,2*S*)-1-(1,3-benzothiazol-2-yl)-1-hydroxy-3-[(3S)-2-oxopyrrolidin-3-yl]propan-2-yl}amino)-4-methyl-1-oxopentan-2-yl]-4-methoxy-1H-indole-2-carboxamide	1.25	[129]
5RHF	1-acetyl-*N*-methyl-*N*-phenylpiperidine-4-carboxamide	1.76	[104]
5RHE	1-acetyl-*N*-(6-methoxypyridin-3-yl)piperidine-4-carboxamide	1.56	[104]
5RGG	4-methyl-*N*-phenylpiperazine-1-carboxamide	2.26	[104]
5RG1	*N*-alpha-acetyl-*N*-(3-bromoprop-2-yn-1-yl)-*L*-tyrosinamide	1.57	[104]
5RGH	5-fluoro-1-[(5-methyl-1,3,4-thiadiazol-2-yl)methyl]-1,2,3,6-tetrahydropyridine	1.70	[104]
5RGR	*N*,1-dimethyl-N-(propan-2-yl)-1H-pyrazolo[3,4-d]pyrimidin-4-amine	1.41	[104]
5RG3	*N* ~ 2 ~ -acetyl-*N* ~ 1 ~ -prop-2-en-1-yl-*L*-aspartamide	1.58	[104]
5RG2	*N* ~ 2 ~ -acetyl-*N*-prop-2-en-1-yl-*D*-allothreoninamide	1.63	[104]
5RGS	[(2~{*R*})-4-(phenylmethyl)morpholin-2-yl]methanol	1.72	[104]
5RGK	2-fluoro-*N*-[2-(pyridin-4-yl)ethyl]benzamide	1.43	[104]
5RGJ	(5*S*)-7-(pyrazin-2-yl)-2-oxa-7-azaspiro[4.4]nonane	1.34	[104]
5RGM	*N*'-acetyl-4,5,6,7-tetrahydro-1-benzothiophene-2-carbohydrazide	2.04	[104]
5RGM	*N*'-acetyl-4,5,6,7-tetrahydro-1-benzothiophene-2-carbohydrazide	2.04	[104]
5RG0	1,1′-(piperazine-1,4-diyl)di(ethan-1-one)	1.72	[104]
5RGN	1-{4-[(4-methylphenyl)sulfonyl]piperazin-1-yl}ethan-1-one	1.86	[104]
5RGQ	1-(4-fluoro-2-methylphenyl)methanesulfonamide	2.15	[104]
5RGP	1-{4-[(2,4-dimethylphenyl)sulfonyl]piperazin-1-yl}ethan-1-one	2.07	[104]
5R8T	–	1.27	[104]
5RGZ	2-(3-cyanophenyl)-*N*-(pyridin-3-yl)acetamide	1.52	[104]
5RHA	1-{4-[(thiophen-2-yl)methyl]piperazin-1-yl}ethan-1-one	1.51	[104]

(*continued on next page*)

Table 2 (*continued*)

PDB ID	Co-crystallized Ligand	Resolution (Å)	Reference
5RH3	(2*R*)-2-(3-chlorophenyl)-*N*-(4-methylpyridin-3-yl)propanamide	1.69	[104]
5RH4	(2*R*)-2-(6-chloro-9H-carbazol-2-yl)propanoic acid	1.34	[104]
5RGU	*N*-(3-{[(2*R*)-4-oxoazetidin-2-yl]oxy}phenyl)-2-(pyrimidin-5-yl)acetamide	2.11	[104]
5RH6	*N*-[(1*R*)-2-[(2-ethyl-6-methylphenyl)amino]-2-oxo-1-(pyridin-3-yl)ethyl]-*N*-[6-(propan-2-yl)pyridin-3-yl]propanamide	1.60	[104]
5RGT	*N*-[(1*R*)-2-(*tert*-butylamino)-2-oxo-1-(pyridin-3-yl)ethyl]-*N*-(5-*tert*-butyl-1,2-oxazol-3-yl)propanamide	2.22	[104]
5RH5	*N*-(5-*tert*-butyl-1,2-oxazol-3-yl)-*N*-[(1*R*)-2-[(4-methoxy-2-methylphenyl)amino]-2-oxo-1-(pyridin-3-yl)ethyl]propanamide	1.72	[104]
5RGW	2-(5-cyanopyridin-3-yl)-N-(pyridin-3-yl)acetamide	1.43	[104]
5RH8	2-(cyanomethoxy)-*N*-[(1,2-thiazol-4-yl)methyl]benzamide	1.81	[104]
5RGV	2-(isoquinolin-4-yl)-*N*-phenylacetamide	1.82	[104]
5RH7	*N*-(5-*tert*-butyl-1H-pyrazol-3-yl)-*N*-[(1R)-2-[(2-ethyl-6-methylphenyl)amino]-2-oxo-1-(pyridin-3-yl)ethyl]propanamide	1.71	[104]
5RGY	*N*-(4-methoxypyridin-2-yl)-2-(naphthalen-2-yl)acetamide	1.976	[104]
5RGX	2-(3-cyanophenyl)-*N*-(4-methylpyridin-3-yl)acetamide	1.69	[104]
5RH9	*N*-{4-[(1*S*)-1-methoxyethyl]phenyl}-*N*-[(1*R*)-2-[(4-methoxy-2-methylphenyl)amino]-2-oxo-1-(pyridin-3-yl)ethyl]propanamide	1.91	[104]
5RH0	*N*-(5-methylthiophen-2-yl)-*N*′-pyridin-3-ylurea	1.92	[104]
5RH2	2-(3-chlorophenyl)-*N*-(4-methylpyridin-3-yl)acetamide	1.83	[104]
5RH1	2-(5-chlorothiophen-2-yl)-*N*-(pyridin-3-yl)acetamide	1.96	[104]
5REA	(azepan-1-yl)(2H-1,3-benzodioxol-5-yl)methanone	1.63	[104]
5REB	1-[(thiophen-3-yl)methyl]piperidin-4-ol	1.68	[104]
5REC	2-{[(1H-benzimidazol-2-yl)amino]methyl}phenol	1.73	[104]
5REE	(2*R*,3*R*)-1-benzyl-2-methylpiperidin-3-ol	1.77	[104]
7JVZ	–	2.50	[130]
6W9Q	–	2.05	[131]
7BRR	(1*S*,2*S*)-2-({*N*-[(benzyloxy)carbonyl]-L-leucyl}amino)-1-hydroxy-3-[(3*S*)-2-oxopyrrolidin-3-yl]propane-1-sulfonic acid	1.40	[132]
7BRO	–	2.00	[133]
7BRP	(1*R*,2*S*,5*S*)-*n*-[(1*S*)-3-amino-1-(cyclobutylmethyl)-2,3-dioxopropyl]-3-[(2*S*)-2-{[(*tert*-butylamino)carbonyl]amino}-3,3-dimethylbutanoyl]-6,6-dimethyl-3-azabicyclo[3.1.0]hexane-2-carboxamide	1.80	[134]
7C2Q	–	1.93	[135]
7C8T	*N*-[(benzyloxy)carbonyl]-*O*-(*tert*-butyl)-l-threonyl-3-cyclohexyl-*N*-[(1*S*)-2-hydroxy-1-{[(3*S*)-2-oxopyrrolidin-3-yl]methyl}ethyl]-l-alaninamide	2.05	[136]
7C8R	Ethyl (4*R*)-4-[[(2*S*)-4-methyl-2-[[(2*S*,3*R*)-3-[(2-methylpropan-2-yl)oxy]-2-(phenylmethoxycarbonylamino)butanoyl]amino]pentanoyl]amino]-5-[(3*S*)-2-oxidanylidenepyrrolidin-3-yl]pentanoate	2.30	[136]
6XCH	–	2.20	[137]
6L70	(1*S*,2*S*)-2-({*N*-[(benzyloxy)carbonyl]-L-leucyl}amino)-1-hydroxy-3-[(3*S*)-2-oxopyrrolidin-3-yl]propane-1-sulfonic acid	1.56	[138]
6FV1	(2~{*S*})-4-methyl-~{*N*}-[(2~{*S*},3~{*R*})-3-oxidanyl-4-oxidanylidene-1-[(3~{*S*})-2-oxidanylidenepyrrolidin-3-yl]-4-[(phenylmethyl)amino]butan-2-yl]-2-[[(~{*E*})-3-phenylprop-2-enoyl]amino]pentanamide	2.30	[139]
6FV2	(*S*)-*N*-benzyl-3-((*S*)-2-cinnamamido-3-phenylpropanamido)-2-oxo-4-((*S*)-2-oxopyrrolidin-3-yl)butanamide	2.95	[139]
7D31	(3~{*S*},3~{a}~{*S*},6~{a}~{*R*})-2-[3-[3,5-bis(fluoranyl)phenyl]propanoyl]-~{*N*}-[(2~{*S*})-1-oxidanylidene-3-[(3~{*S*})-2-oxidanylidenepyrrolidin-3-yl]propan-2-yl]-3,3~{a},4,5,6,6~{a}-hexahydro-1~{H}-cyclopenta[c]pyrrole-3-carboxamide 2	2.00	[140]
7D1O	(1*R*,2*S*,5*S*)-3-[*N*-({1-[(*tert*-butylsulfonyl)methyl]cyclohexyl}carbamoyl)-3-methyl-*L*-valyl]-*N*-{(1*S*)-1-[(1*R*)-2-(cyclopropylamino)-1-hydroxy-2-oxoethyl]pentyl}-6,6-dimethyl-3-azabicyclo[3.1.0]hexane-2-carboxamide	1.78	[141]
7C7P	(1*S*,3a*R*,6a*S*)-2-[(2*S*)-2-({(2*S*)-2-cyclohexyl-2-[(pyrazin-2-ylcarbonyl)amino]acetyl}amino)-3,3-dimethylbutanoyl]-*N*-[(2*R*,3*S*)-1-(cyclopropylamino)-2-hydroxy-1-oxohexan-3-yl]octahydrocyclopenta[c]pyrrole-1-carboxamide (3~{*S*},3~{a}~{*S*},6~{a}~{*R*})-~{*N*}-[(2~{*R*},3~{S})-1-(cyclopropylamino)-2-oxidanyl-1-oxidanylidene-hexan-3-yl]-2-methanoyl-3,3~{a},4,5,6,6~{a}-hexahydro-1~{H}-cyclopenta[c]pyrrole-3-carboxamide	1.74	[142]
7COM	boceprevir (bound form)	2.25	[143]
6ZRU	boceprevir (bound form)	2.10	[144]
6ZRT	(1*S*,3a*R*,6a*S*)-2-[(2*S*)-2-({(2*S*)-2-cyclohexyl-2-[(pyrazin-2-ylcarbonyl)amino]acetyl}amino)-3,3-dimethylbutanoyl]-*N*-[(2*R*,3*S*)-1-(cyclopropylamino)-2-hydroxy-1-oxohexan-3-yl]octahydrocyclopenta[c]pyrrole-1-carboxamide	2.10	[145]
6MOK	–	5.10	[146]
6LZE	~{*N*}-[(2~{*S*})-3-cyclohexyl-1-oxidanylidene-1-[[(2~{*S*})-1-oxidanylidene-3-[(3~{*S*})-2-oxidanylidenepyrrolidin-3-yl]propan-2-yl]amino]propan-2-yl]-1~{H}-indole-2-carboxamide	1.50	[147]
7C6S	boceprevir (bound form)	1.60	[148]
7CX9	3-iodanyl-1~{H}-indazole-7-carbaldehyde	1.73	[149]

bearing hexylcarbamide acid structure, in which the fatty acid tail occupies the hydrophobic S2 sub-site. A study reported that carmofur inhibits viral replication in cells (EC_{50} = 24.30 μM) and is a promising lead compound to develop a new antiviral treatment for SARS-Coronavirus-2.

A more diverse inhibitor's structure was observed from the 3D-crystal structure with PDB ID 5RGG which was resolved at 2.26 Å of resolution [104]; Fig. 7c). The inhibitor is a carboxamide derivative namely 4-methyl-*N*-phenylpiperazine-1-carboxamide, binds at HIS80 via H-bond interaction. Instead of H-bond, HIS80 was also interacting with the inhibitor via hydrophobic interaction which was co-bound with LYS90. This experiment could give an insight into understanding that even a small molecule is able to bind the protease. However, the potency of such inhibitor could be low due to the larger cavities which need an extending occupation.

6. Biflavonoid as the protease –Inhibitor

There are a few studies of biflavonoid-class compounds reporting their activities as protease inhibitors. Amentoflavone from *Torreya nucifera* was the early biflavonoid studied in its inhibitory activity against SARS-Coronavirus 3CLpro by showing IC_{50} 8.3 μM. The results were compared to three types of flavonoid (apigenin, luteolin, and quercetin) which showed less inhibition and therefore, the structure–activity relationships were generated to confirm that the more potent activity of biflavonoid appeared to be associated with the presence of benzene ring moiety at C-3′ position of flavones, as biflavone affected 3CLpro inhibitory activity [36].

Based on Ryu et al. findings, a QSAR study of biflavonoid and its analogs was carried out to generate a QSAR model defining the increasing value of the dipole moment along the X-axis that may be

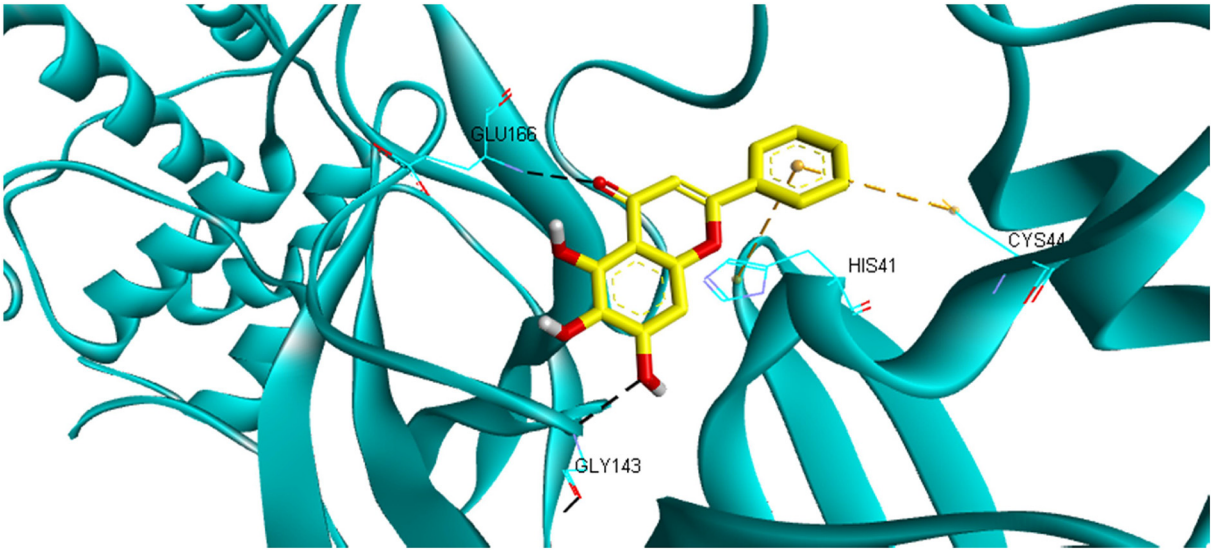

Fig. 5. The interaction between 5,6,7-trihydroxy-2-phenyl-4H-chromen-4-one and the active site of SARS-Coronavirus-2 (PDB ID 6M2N). The 3CLpro is presented in a blue ribbon model, whereas the inhibitor is in a stick model (yellow = C, white = H, and red = O). The H-bond and hydrophobic interactions are presented in black and yellow dot lines, respectively. (For interpretation of the references to colour in this figure legend, the reader is referred to the web version of this article.)

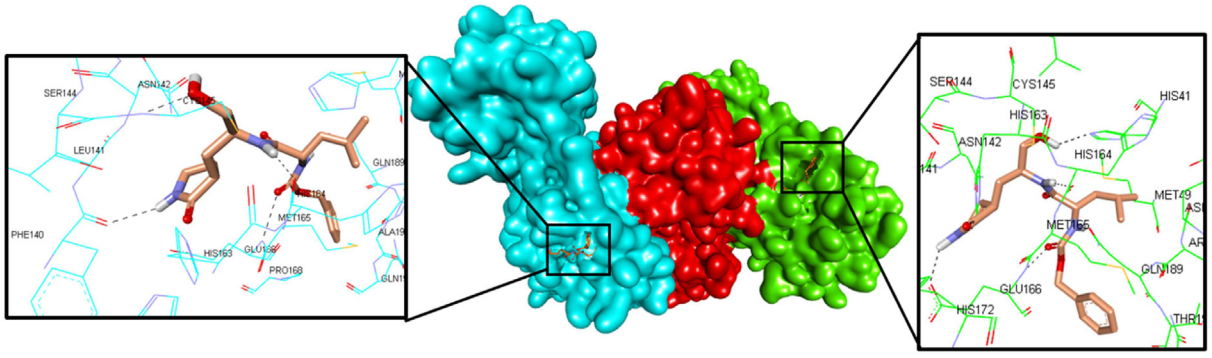

Fig. 6. The trimer structure of 3CLpro as indicated by blue (monomer A), red (monomer B), and green (monomer C) surface models. Inset is the ligand complex to the active site of the enzyme (presented by blue stick and green stick, for monomer A and monomer C, respectively), presented in a stick model (orange = C, white = H, blue = N and red = O). The H-bond is presented in black dot lines, respectively. (For interpretation of the references to colour in this figure legend, the reader is referred to the web version of this article.)

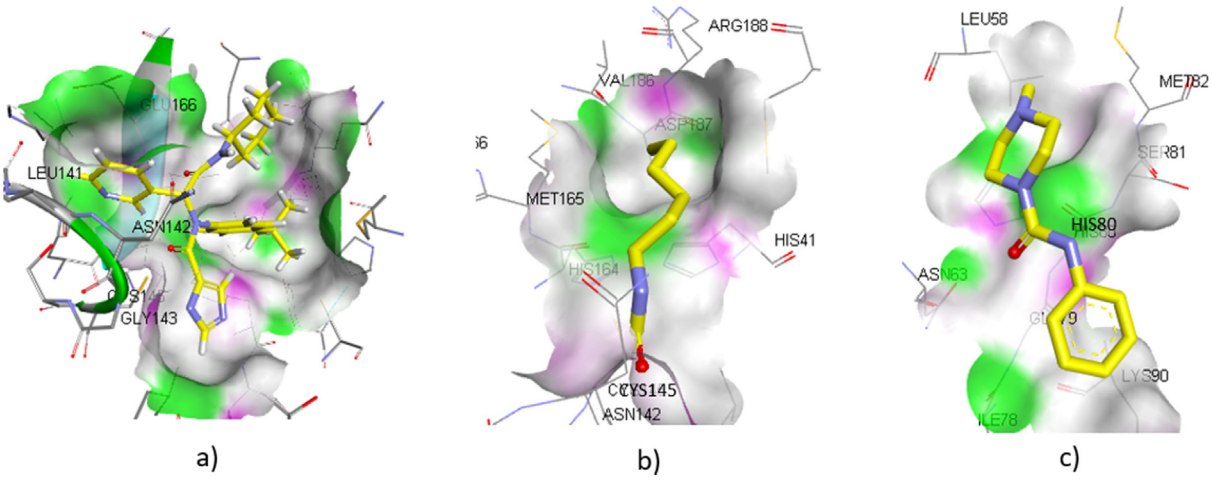

Fig. 7. The presentation of a) imidazole-4-carboxamide, b) carmofur, and c) 4-methyl-*N*-phenylpiperazine-1-carboxamide bound into the active site of SARS-Coronavirus-2 3CLpro. The protein is visualized in the surface model with the green area = hydrogen bond acceptor residues, white area = neutral residues, and magenta area = hydrogen bond donor residues. The ligands are presented in a stick form with yellow = C, white = H, blue = N, and red = O. (For interpretation of the references to colour in this figure legend, the reader is referred to the web version of this article.)

conducive to the activity. Therefore, the steric character of this part may be favorable for its activity. Compounds having higher dipole moment due to the much bulky aryl groups, therefore, have a higher activity than the compound having less bulky aryl group [23].

The antiproteolytic activity of biflavonoid was determined early on morelloflavone-4‴-*O*-*β*-*D*-glycosyl, (±)-fukugiside, and morelloflavone. These biflavonoids were isolated from the fruit epocarp of *Garcinia brasiliensis* which were further semi synthesized into three moreflavone derivatives i.e. morelloflavone-7,4′,7″,3‴,4′‴- penta-*O*-acetyl, morelloflavone-7,4′,7″,3‴,4‴-penta-*O*-methyl, and morelloflavone-7,4′,7″,3‴,4‴-penta-*[*-butanoyl. High inhibitory activity was demonstrated by this biflavonioid against r-CPB2.8 and r-CPB3 isoforms which are papain-like protease of *Leismania mexicana* with IC_{50} 0.42–1.01 μM for the four most active compounds. Interestingly, there was no cytotoxic activity towards the normal cell lines as observed from the *in vitro* study [150].

Further study was pursued by the same research group in evaluating those biflavonoid activities against the cysteine protease (papain and cruzain) and serine protease of *Trypanozoma cruzii*. All biflavonoid compounds demonstrated excellent inhibitions toward all protease enzymes (IC_{50} 0.02–106 μM). However, morelloflavone-7,4′,7″,3‴,4‴′- penta-*O*-acetyl showed the best activity which might be due to the carbonyl group in the structure. This functional group could favor a higher nucleophilic attack by serine and cysteine proteases. This is in accordance with morelloflavone-7,4′,7″,3‴,4‴-penta-*O*-methyl (IC_{50} = 15.4 ± 0.7 μM for papain), in which the compound having no carbonyl group in structure was less active in the inhibition process. This was confirmed by the structure–activity relationships (SARs) study which had been performed using flexible docking simulations [151].

A study by Assis et al. reported that fukugetin, a biflavone originated from *Garcinia brasiliensis*, demonstrated partial competitive and hyperbolic-mix type inhibitions against the major cysteine protease of *Trypanosoma cruzii* (cruzain and papain), respectively. The potency of such biflavone was expressed in a slowly reversible type of inhibition with Ki 1.1 and 13.4 μM for cruzain and papain, respectively, describing that the biflavone has 12 times faster inhibition toward cruzain than papain in inhibiting the enzymes. The molecular docking study predicted that this activity is due to the chemical interaction between biflavone at ring C with S3 pocket, whereas the ring C' binds at S2 pocket through hydrogen bonds as well as the hydrophobic interactions [152].

Virtual screening was performed to identify the hits of the tryptase inhibitor followed by *in vitro* experiments to identify the lead compounds. Tryptase is a class of serine protease enzyme released as the allergic response such as skin inflammation and asthma from the mast cells. Out of the 98,000 compounds screened, 2.28% of the library (2503 compounds) were selected as the hits. Interestingly, biflavonoids were one of the most frequently represented in the 200 compounds with the strongest tryptase binding energy. Using fluorescence resonane energy transfer (FRET)-based assay, these 200 compounds were further *in vitro* screened to afford the lead compound, and then the biflavonoid podocorpus flavone A blocks the tryptase activity by 61.6.%. The docking study suggested that the biflavonoid is favorably binding at the S4 of tryptase [153].

Biflavonoid was also reported to down-regulate the expression of matrix metalloproteinase-1 (MMP-1) from human skin fibroblasts. MMP is a zymogen (zinc-dependent peptidase) that degrades the extracellular matrix to perform angiogenesis, inflammation, cell migration, and tissue remodeling. The high expression of this enzyme is often associated with cancer and wound diabetic foot ulcers. 2′,8″-biapigenin, sumaflavone, taiwaniaflavone, amentoflavone, and robustaflavone which were isolated from *Selaginella tamariscina* showed significant MMP-1 inhibitory activity in primary human dermal fibroblasts after UV irradiation. The IC_{50} values of sumaflavone, amentoflavone, and retinoic acid (used as the positive control) were 0.78, 1.8, and 10 μM, respectively [154].

7. Perspectives

Two main protein targets in the coronaviral genome are classified into structural and non-structural proteins. Structural protein which is composed of the membrane, envelope and nucleocapsid is formed in the inner viral cell, whereas the spike protein is located in the outer cell [155,156]. It might be difficult to control the activity of such structural protein because they control the virus's life during the viral cell assembly which could be too fast to control. Most likely, the host will be suddenly infected by the virus while there is no time to block the activity of the S protein during viral-host attachment as well as its endocytosis. Therefore, in designing the protein inhibitor for coronavirus, the non-structural protein could be more favorable than the structural protein due to its role in controlling the polypeptide proteolytic, reverse transcription, RNA replication as well as protein translation, which might take more time than the viral assembly.

Among the 16 non-structural proteins, NSP5 is the most attractive target while the others are still elusive [157]. The NSP5 main protease (3CLpro) is the most common targeted protein in coronavirus because it is formed in the host and acts during cleavage and post-translational polyprotein synthesis. Thus, it is relatively easier to control their activities. Two classes of the compound are reported to have these protein activities, including peptide and non-peptide compound. Naturally, the protease has a peptide substrate due to its function to hydrolyze the peptide bond upon proteolysis. Therefore, for a competitive inhibitor, a compound having a peptide-like structure should be suitable to block the enzyme-substrate binding. There are notable peptide (like) compounds demonstrating low micromolar activity towards the protease such as lopinavir and ritonavir [158].

Although peptide is the suitable structure designed for the protease inhibitor, however, the physic-chemical properties of this class of compound often make it fails under clinical trials. The peptide has a number of flexible bonds which makes it energetically unstable either during preparation or the pharmacokinetic stage. The structure is mimicking protein, therefore, it is sensitive towards denaturation and hydrolysis during preparation. At the pharmacokinetic stage especially during absorption, the peptide is less absorbed due to its isoelectric character which makes it very polar in aqueous biological fluids. Thus, it is hard to penetrate the intestinal membrane lipid bilayer [159]. This causes the peptide to become unsuitable for oral preparation which requires the absorption process.

Another alternative is formulated in the parenteral preparation. However, this is costly and not applicable to be administered by the patient. Therefore, the peptide is practically used as the model only and then should be further modified to the more rigid character to improve the stability. One effort has been conducted to formulate the drug delivery system to improve bioavailability such as using liposome technology. However, the use of organic solvents in the liposome dosage form could make it toxic [160,161].

Non-peptide or often called as small molecule inhibitors currently takes more attention used as the molecule target for protease inhibitors. The presence of aromatic rings could make the compound energetically more stable than the peptide due to its rigid character [162]. The rigid character causes less entropy of the compound and thus stabilizes the compound-enzyme affinity upon binding [163]. The non-peptide inhibitor can still be divided into natural and synthetic compounds. Natural compound is a unique structure due to the presence of chiral carbon which could make the ligand–protein binding more specific. A class of biflavonoid showed the *in vitro* competitive inhibition in low micromolar activities towards the protease which agreed with the docking explanation. Amentoflavone is the

early biflavonoid found active against 3CLpro of SARS-Coronavirus underlining the potency of such compounds to be this protease inhibitor. It was postulated that the presence of benzene ring moiety is at position C-3′ of flavones, as biflavone affected 3CLpro inhibitory activity. The synthetic (semi-synthetic) biflavonoids are the further strategy to get the product being more feasible to be developed as a protease inhibitor. Compounds bearing more carbonyl groups seem promising to be the protease inhibitor as it is designed to favor a higher nucleophilic attack by serine and cysteine proteases using molecular docking. The complex of 5,6,7-trihydroxy-2-phenyl-4H-chromen-4-one with SARS-Coronavirus-2 3CLpro (PDB ID 6M2N) is one of the proofs that flavonoid is such an important feature for 3CLpro pharmacophore and so does the biflavonoid which could cover more space to interact with the 3CLpro.

3CLpro is still the most recommended protein target in the discovery of anti-SARS coronaviral agents. The availability of crystal structure and its high conserved binding site make the structure-based drug design becomes applicable [164,165]. The structure-based drug design can also be combined with ligand-based drug design since the structure information of the compounds either in peptide or non-peptide has been reported as the protease inhibitors. The non-peptide compound such as biflavonoid provides more promising candidate to enter either pre- or clinical stage due to its more stable physicchemical properties during preparation as well as pharmacokinetics.

8. Conclusion

In conclusion, our review strongly recommends that biflavonoid, either from the natural product or its synthetic is very potential to be used as of SARS-Coronavirus-2 3CLpro inhibitor. Its dimer and big structure are more suitable for a 3CLpro binding site composing two beta barrels than the corresponding flavones. To the best of our knowledge, this is the first review to describe the potential inhibitory effects of biflavonoid against SARS-Coronavirus-2 3CLpro. Thus, we believe that this compound may be a good candidate for development as a natural therapeutic drug against SARS-Coronavirus-2 infection.

CRediT authorship contribution statement

Yustina Hartini: Writing. **Bakti Saputra:** Writing. **Bryan Wahono:** Writing. **Zerlinda Auw:** Writing. **Friska Indayani:** Writing. **Lintang Adelya:** Writing. **Gabriel Namba:** Writing. **Maywan Harionо:** Conceptualization, Editing.

Declaration of Competing Interest

The authors declare that they have no known competing financial interests or personal relationships that could have appeared to influence the work reported in this paper.

Acknowledgement

MH show profound gratitude to Lembaga Penelitian dan Pengabdian Masyarakat (LPPM) Sanata Dharma University under special scheme “Covid-19”, No. 035/Penel./LPPM-USD/III/2019 for their financial support.

References

[1] R. Djalante, J. Lassa, D. Setiamarga, C. Mahfud, A. Sudjatma, M. Indrawan, L.A. Gunawan, Review and analysis of current responses to COVID-19 in Indonesia: Period of January to March 2020, Prog Disaster Sci 6 (2020), https://doi.org/10.1016/j.pdisas.2020.100091 100091.

[2] World Health Organization. WHO coronavirus disease (covid-19) dashboard, https://covid19.who.int/; 2020 (accessed 24 October 2020).

[3] Kompas.com, Data covid-19 di Indonesia, https://www.kompas.com/covid-19; 2020 (accessed 24 October 2020).

[4] United Nations Industrial Development Organization, Corionavirus, the economic impact-10 July 2020, https://www.unido.org/stories/coronavirus-economic-impact-10-july-2020; 2020 (accessed 24 October 2020).

[5] K. Dhama, S.K. Patel, K. Sharun, M. Pathak, R. Tiwari, M.I. Yatoo, K.P. Singh, SARS-CoV-2 jumping the species barrier: zoonotic lessons from SARS, MERS and recent advances to combat this pandemic virus, Travel Med. Infect. Dis. 37 (2020), https://doi.org/10.1016/j.tmaid.2020.101830 101830.

[6] E.S. Hosseini, N.R. Kashani, H. Nikzad, J. Azadbakht, H.H. Bafrani, H.H. Kashani, The novel coronavirus Disease-2019 (COVID-19): Mechanism of action, detection and recent therapeutic strategies, Virology 551 (2020) 1–9, https://doi.org/10.1016/j.virol.2020.08.011.

[7] N. Prasad, N. Gopalakrishnan, M. Sahay, A. Gupta, S.K. Agarwal, Epidemiology, genomic structure, the molecular mechanism of injury, diagnosis and clinical manifestations of coronavirus infection: An overview, Indian J Nephrol 30 (2020) 143, https://doi.org/10.4103/ijn.IJN_191_20.

[8] E.J. Snijder, E. Decroly, J. Ziebuhr, The nonstructural proteins directing coronavirus RNA synthesis and processing, Adv. Virus Res. 96 (2016) 59–126, https://doi.org/10.1016/bs.aivir.2016.08.008.

[9] M.A. Shereen, S. Khan, A. Kazmi, N. Bashir, R. Siddique, COVID-19 infection: Origin, transmission, and characteristics of human coronaviruses, J. Adv. Res. 24 (2020) 91–98, https://doi.org/10.1016/j.jare.2020.03.005.

[10] V. Grum-Tokars, K. Ratia, A. Begaye, S.C. Baker, A.D. Mesecar, Evaluating the 3C-like protease activity of SARS-Coronavirus: recommendations for standardized assays for drug discovery, Virus Res. 133 (2008) 63–73, https://doi.org/10.1016/j.virusres.2007.02.015.

[11] S. Joshi, M. Joshi, M.S. Degani, Tackling SARS-CoV-2: proposed targets and repurposed drugs, Future Med. Chem. 12 (2020) 1579–1601, https://doi.org/10.4155/fmc-2020-0147.

[12] Y.M. Báez-Santos, S.E.S. John, A.D. Mesecar, The SARS-coronavirus papain-like protease: structure, function and inhibition by designed antiviral compounds, Antivir Res 115 (2015) 21–38, https://doi.org/10.1016/j.antiviral.2014.12.015.

[13] R.M.L. Colunga Biancatelli, M. Berrill, J.D. Catravas, P.E. Marik, Quercetin and vitamin C: an experimental, synergistic therapy for the prevention and treatment of SARS-CoV-2 related disease (COVID-19), Front. Immunol. 11 (2020) 1451, https://doi.org/10.3389/fimmu.2020.01451.

[14] K. Chojnacka, A. Witek-Krowiak, D. Skrzypczak, K. Mikula, P. Młynarz, Phytochemicals containing biologically active polyphenols as an effective agent against Covid-19-inducing coronavirus, J. Funct. Foods 73 (2020), https://doi.org/10.1016/j.jff.2020.104146 104146.

[15] R. Jain, S. Shukla, N. Nema, A. Panday, H.S. Gour, A systemic review: structural mechanism of SARS-CoV-2A and promising preventive cure by phytochemicals, Int. J. Immunol. Immunother. 7 (2020) 051, https://doi.org/10.23937/2378-3672/1410051.

[16] S.Y. Li, C. Chen, H.Q. Zhang, H.Y. Guo, H. Wang, L. Wang, R.S. Li, Identification of natural compounds with antiviral activities against SARS-associated coronavirus, Antivir. Res. 67 (2005) 18–23, https://doi.org/10.1016/j.antiviral.2005.02.007.

[17] C.W. Lin, F.J. Tsai, C.H. Tsai, C.C. Lai, L. Wan, T.Y. Ho, P.D.L. Chao, Anti-SARS coronavirus 3C-like protease effects of Isatis indigotica root and plant-derived phenolic compounds, Antivir. Res. 68 (2005) 36–42, https://doi.org/10.1016/j.antiviral.2005.07.002.

[18] S. Schwarz, D. Sauter, K. Wang, R. Zhang, B. Sun, A. Karioti, W. Schwarz, Kaempferol derivatives as antiviral drugs against the 3a channel protein of coronavirus, Planta Med. 80 (2014) 177. 10.1055%2Fs-0033-1360277.

[19] J. Cinatl, B. Morgenstern, G. Bauer, P. Chandra, H. Rabenau, H.W. Doerr, Glycyrrhizin, an active component of liquorice roots, and replication of SARS-associated coronavirus, Lancet 361 (2003) 2045–2046, https://doi.org/10.1016/S0140-6736(03)13615-X.

[20] D.E. Kim, J.S. Min, M.S. Jang, J.Y. Lee, Y.S. Shin, C.M. Park, S. Kwon, Natural bis-benzylisoquinoline alkaloids-tetrandrine, fangchinoline, and cepharanthine, inhibit human coronavirus OC43 infection of MRC-5 human lung cells, Biomolecules 9 (2019) 696, https://doi.org/10.3390/biom9110696.

[21] C. Müller, F.W. Schulte, K. Lange-Grünweller, W. Obermann, R. Madhugiri, S. Pleschka, A. Grünweller, Broad-spectrum antiviral activity of the eIF4A inhibitor silvestrol against corona-and picornaviruses, Antivir Res 150 (2018) 123–129, https://doi.org/10.1016/j.antiviral.2017.12.010.

[22] A.T. Jamiu, C.E. Aruwa, I.A. Abdulakeem, A.A. Ajao, S. Sabiu, Phytotherapeutic Evidence Against Coronaviruses and Prospects for COVID-19, Pharmacogn J 12 (2020) 1252–1257, https://doi.org/10.5530/pj.2020.12.174.

[23] Adhikari N, Baidya SK, Saha A, Jha T. Structural Insight Into the Viral 3C-Like Protease Inhibitors: Comparative SAR/QSAR Approaches. In Viral Proteases and Their Inhibitors 2017 (pp. 317-409). Academic Press. https://doi.org/10.1016/B978-0-12-809712-0.00011-3

[24] E. Di Cera, Serine proteases. IUBMB life 61 (2009) 510–515, https://doi.org/10.1002/iub.186.

[25] Geiger H, Quinn C. Biflavonoids. In The flavonoids 1975 (pp. 692-742). Springer, Boston, MA. https://doi.org/10.1007/978-1-4899-2909-9_13

[26] A.B. GMercader, A. Pomilio, Naturally-occurring dimers of flavonoids as anticarcinogens, Anti-Cancer Agents Med. Chem. 13 (2013) 1217–1235, https://doi.org/10.2174/18715206113139990300.

[27] A.N. Panche, A.D. Diwan, S.R. Chandra, Flavonoids: an overview, J Nutr Sci 5 (2016) 1–15, https://doi.org/10.1017/jns.2016.41.

[28] J.B. Harborne, H. Marby, T.J. Marby, The flavonoids, Springer, 2013. https://doi.org/10.1007/978-1-4899-2909-9.

[29] P.G. Pietta, Flavonoids as antioxidants, J. Nat. Prod. 63 (2000) 1035–1042, https://doi.org/10.1021/np9904509.

[30] T.T. Cushnie, A.J. Lamb, Antimicrobial activity of flavonoids, Int. J. Antimicrob. Agents 26 (2005) 343–356, https://doi.org/10.1016/j.ijantimicag.2005.09.002.
[31] Mabry T, Markham KR, Thomas, MB. The systematic identification of flavonoids. Springer Science & Business Media. 1st Ed. Berlin-Heidelberg; Springer verlag: 1970. https://doi.org/10.1007/978-3-642-88458-0
[32] R.N. Oliveira, M.C. Mancini, F.C.S.D. Oliveira, T.M. Passos, B. Quilty, R.M.D.S.M. Thiré, G.B. McGuinness, FTIR analysis and quantification of phenols and flavonoids of five commercially available plants extracts used in wound healing, Matéria 21 (2016) 767–779, https://doi.org/10.1590/S1517-707620160003.0072.
[33] R. March, J. Brodbelt, Analysis of flavonoids: tandem mass spectrometry, computational methods, and NMR, J. Mass Spectrom. 43 (2008) 1581–1617, https://doi.org/10.1002/jms.1480.
[34] M. Okigawa, N. Kawano, The structure of ochnaflavone, a new type of biflavone and the synthesis of its pentamethyl ether, Tetrahed Lett 22 (1973) 2003, https://doi.org/10.1016/S0040-4039(01)96104-0.
[35] K.H. Son, J.O. Park, K.C. Chung, H.W. Chang, H.P. Kim, J.S. Kim, S.S. Kang, Triterpenoid saponins from the aerial parts of Lonicera japonica, Arch Pharm Res 15 (1994) 365, https://doi.org/10.1016/S0031-9422(00)90656-3.
[36] Y.B. Ryu, H.J. Jeong, J.H. Kim, Y.M. Kim, J.Y. Park, D. Kim, M.C. Rho, Biflavonoids from Torreya nucifera displaying SARS-CoV 3CLpro inhibition, Bioorg. Med. Chem. 18 (2010) 7940–7947, https://doi.org/10.1016/j.bmc.2010.09.035.
[37] S. Yu, H. Yan, L. Zhang, M. Shan, P. Chen, A. Ding, S.F.Y. Li, A review on the phytochemistry, pharmacology, and pharmacokinetics of amentoflavone, a naturally-occurring biflavonoid, Molecules 22 (2017) 299, https://doi.org/10.3390/molecules22020299.
[38] M.M. Feuereisen, M.G. Barraza, B.F. Zimmermann, A. Schieber, N. Schulze-Kaysers, Pressurized liquid extraction of anthocyanins and biflavonoids from Schinus terebinthifolius Raddi: A multivariate optimization, Food Chem. 214 (2017) 564–571, https://doi.org/10.1016/j.foodchem.2016.07.002.
[39] M.J. Waterman, A.S. Nugraha, R. Hendra, G.E. Ball, S.A. Robinson, P.A. Keller, Antarctic moss biflavonoids show high antioxidant and ultraviolet-screening activity, J. Nat. Prod. 80 (2017) 2224–2231, https://doi.org/10.1021/acs.jnatprod.7b00085.
[40] D. Li, Y. Qian, Y.J. Tian, S.M. Yuan, W. Wei, G. Wang, Optimization of ionic liquid-assisted extraction of biflavonoids from Selaginella doederleinii and evaluation of its antioxidant and antitumor activity, Molecules 22 (2017) 586, https://doi.org/10.3390/molecules22040586.
[41] N. Chatsumpun, B. Sritularak, K. Likhitwitayawuid, New biflavonoids with α-glucosidase and pancreatic lipase inhibitory activities from Boesenbergia rotunda, Molecules 22 (2017) 1862, https://doi.org/10.3390/molecules22111862.
[42] J.H. Tabares-Guevara, O.J. Lara-Guzmán, J.A. Londoño-Londoño, J.A. Sierra, Y. M. León-Varela, R.M. Álvarez-Quintero, J.R. Ramirez-Pineda, Natural Biflavonoids Modulate Macrophage-Oxidized LDL Interaction In Vitro and Promote Atheroprotection In Vivo, Front. Immunol. 8 (2017) 923, https://doi.org/10.3389/fimmu.2017.00923.
[43] P. Li, G.G.L. Yue, H.F. Kwok, C.L. Long, C.B.S. Lau, E.J. Kennelly, Using ultra-performance liquid chromatography quadrupole time of flight mass spectrometry-based chemometrics for the identification of anti-angiogenic biflavonoids from edible Garcinia species, J. Agric. Food Chem. 65 (2017) 8348–8355, https://doi.org/10.1021/acs.jafc.7b02867.
[44] P. Gürbüz, Ş.D. Doğan, Biflavonoids from Fumana procumbens (Dunal), Gren. & Godr. Biochem Syst Ecol 74 (2017) 57–59, https://doi.org/10.1016/j.bse.2017.09.004.
[45] Recalde-Gil MA, Klein-Júnior LC, dos Santos Passos C, Salton J, de Loreto Bordignon SA, Monace FD, Henriques AT. Monoamine oxidase inhibitory activity of biflavonoids from branches of Garcinia gardneriana (Clusiaceae). Nat Prod Commun 2017; 12: 1934578X1701200411. https://doi.org/10.1177%2F1934578X1701200411
[46] F.A. Adem, A.T. Mbaveng, V. Kuete, M. Heydenreich, A. Ndakala, B. Irungu, T. Efferth, Cytotoxicity of isoflavones and biflavonoids from Ormocarpum kirkii towards multi-factorial drug resistant cancer, Phytomedicine 58 (2019), https://doi.org/10.1016/j.phymed.2019.152853 152853.
[47] M. Li, B. Li, Z.M. Xia, Y. Tian, D. Zhang, W.J. Rui, F.J. Xiao, Anticancer effects of five biflavonoids from Ginkgo Biloba L. male flowers in vitro, Molecules 24 (2019) 1496, https://doi.org/10.3390/molecules24081496.
[48] L.I. Yun-Ying, L.U. Xiao-Yan, S.U.N. Jia-Li, W.A.N.G. Qing-Qing, Y.D. Zhang, J.B. Zhang, F.A.N. Xiao-Hui, Potential hepatic and renal toxicity induced by the biflavonoids from Ginkgo biloba, Chin. J. Nat. Med. 17 (2019) 672–681, https://doi.org/10.1016/S1875-5364(19)30081-0.
[49] M. Linden, C. Brinckmann, M.M. Feuereisen, A. Schieber, Effects of structural differences on the antibacterial activity of biflavonoids from fruits of the Brazilian peppertree (Schinus terebinthifolius Raddi), Food Res. Int. 133 (2020), https://doi.org/10.1016/j.foodres.2020.109134 109134.
[50] J. Xu, L. Yang, R. Wang, K. Zeng, B. Fan, Z. Zhao, The biflavonoids as protein tyrosine phosphatase 1B inhibitors from Selaginella uncinata and their antihyperglycemic action, Fitoterapia 137 (2019), https://doi.org/10.1016/j.fitote.2019.104255 104255.
[51] Mendiratta A, Dayal R, Bartley JP, Smith G. A Phenylpropanoid and Biflavonoids from the Needles of Cephalotaxus harringtonia var. harringtonia. Nat Prod Commun 2017; 12: 1934578X1701201132. https://doi.org/10.1177%2F1934578X1701201132
[52] Oliveira PDA, Fidelis QC, Fernandes TFDC, Souza MCD, Coutinho DM, Prudêncio ER, Marinho BG. Evaluation In Vivo and In Vitro of the Antioxidant, Antinociceptive, and Anti-Inflammatory Activities of Biflavonoids From Ouratea hexasperma and O. ferruginea. Nat Prod Commun 2019; 14: 1934578X19856802. https://doi.org/10.1177%2F1934578X19856802
[53] N. Sirimangkalakitti, L.D. Juliawaty, E.H. Hakim, I. Waliana, N. Saito, K. Koyama, K. Kinoshita, Naturally occurring biflavonoids with amyloid β aggregation inhibitory activity for development of anti-Alzheimer agents, Bioorg. Med. Chem. Lett. 29 (2019) 1994–1997, https://doi.org/10.1016/j.bmcl.2019.05.020.
[54] H.W. Yan, H. Zhu, X. Yuan, Y.N. Yang, Z.M. Feng, J.S. Jiang, P.C. Zhang, Eight new biflavonoids with lavandulyl units from the roots of Sophora flavescens and their inhibitory effect on PTP1B, Bioorg. Chem. 86 (2019) 679–685, https://doi.org/10.1016/j.bioorg.2019.01.058.
[55] G.A. Dziwornu, N.R. Toorabally, M.G. Bhowon, S. Jhaumeer-Laulloo, S. Sunassee, A. Moser, D. Argyropoulos, Computer Assisted Structure Elucidation of Two Biflavonoids from the Leaves of Ochna Mauritiana, Plant Med. Int. Open 4 (2017) Mo-PO, https://doi.org/10.1055/s-0037-1608237.
[56] I. Abdullah, S. Phongpaichit, S.P. Voravuthikunchai, W. Mahabusarakam, Prenylated biflavonoids from the green branches of Garcinia dulcis, Phytochem. Lett. 23 (2018) 176–179, https://doi.org/10.1016/j.phytol.2017.12.004.
[57] D. Ren, F.C. Meng, H. Liu, T. Xiao, J.J. Lu, L.G. Lin, Q.W. Zhang, Novel biflavonoids from Cephalotaxus oliveri Mast, Phytochem. Lett. 24 (2018) 150–153, https://doi.org/10.1016/j.phytol.2018.02.005.
[58] X. Zhang, R. Gao, Y. Liu, Y. Cong, D. Zhang, Y. Zhang, C. Lu, Anti-virulence activities of biflavonoids from Mesua ferrea L. flower, Drug Discov. Ther. 13 (2019) 222–227, https://doi.org/10.5582/ddt.2019.01053.
[59] L. Carrillo-Hormaza, A.M. Ramírez, C. Quintero-Ortiz, M. Cossio, S. Medina, F. Ferreres, E. Osorio, Comprehensive characterization and antioxidant activities of the main biflavonoids of Garcinia madruno: A novel tropical species for developing functional products, J Funct Food 27 (2016) 503–516, https://doi.org/10.1016/j.jff.2016.10.001.
[60] H. Jin, H. Cui, X. Yang, L. Xu, X. Li, R. Liu, X. Song, Nematicidal activity against Aphelenchoides besseyi and Ditylenchus destructor of three biflavonoids, isolated from roots of Stellera chamaejasme, J. Asia Pac. Entomol. 21 (2018) 1473–1478, https://doi.org/10.1016/j.aspen.2018.11.013.
[61] S. Xiao, Z.Q. Mu, C.R. Cheng, J. Ding, Three new biflavonoids from the branches and leaves of Cephalotaxus oliveri and their antioxidant activity, Nat. Prod. Res. 33 (2019) 321–327, https://doi.org/10.1080/14786419.2018.1448817.
[62] K. Zar Wynn Myint, T. Kido, K. Kusakari, H. Prasad Devkota, T. Kawahara, T. Watanabe, Rhusflavanone and mesuaferrone B: tyrosinase and elastase inhibitory biflavonoids extracted from the stamens of Mesua ferrea L, Nat. Prod. Res. (2019) 1–5, https://doi.org/10.1080/14786419.2019.1613395.
[63] Y. Sun, B. Shi, M. Gao, L. Fu, H. Chen, Z. Hao, W. Feng, Two New Biflavonoids from the Roots and Rhizomes of Sinopodophyllum emodi, Chem. Nat. Compd. 54 (2018) 649–653, https://doi.org/10.1007/s10600-018-2438-4.
[64] Y. Liu, N. Kelsang, J. Lu, Y. Zhang, H. Liang, P. Tu, Q. Zhang, Oxytrodiflavanone A and Oxytrochalcoflavanones A, B: New Biflavonoids from Oxytropis chiliophylla, Molecules 24 (2019) 1468, https://doi.org/10.3390/molecules24081468.
[65] D. Li, C. Sun, J. Yang, X. Ma, Y. Jiang, S. Qiu, G. Wang, Ionic liquid-microwave-based extraction of biflavonoids from Selaginella sinensis, Molecules 24 (2019) 2507, https://doi.org/10.3390/molecules24132507.
[66] M. Ndoile, F. Van Heerden, Cytotoxic and antimalarial biflavonoids isolated from the aerial parts of Ochna serrulata (Hochst.) Walp, Tanzania J. Sci. 44 (2018) 152–162.
[67] E.A. Ibrahim, S.Y. Desoukey, G.M. Hadad, R.A. Salam, A.K. Ibrahim, S.A. Ahmed, M.A. ElSohly, Analysis of cupressuflavone and amentoflavone from Cupressus sempervirens L. and its tissue cultured callus using HPLC-DAD method, Pharm. Pharmacol. Int. J. 5 (2017) 174–180.
[68] T. Sabudak, M. Ozturk, E. Alpay, New Bioflavonoids from Solanum nigrum L. by anticholinesterase and anti-tyrosinase activities-guided fractionation, Rec. Nat. Prod. 1 (2017) 130–140.
[69] S.Y. Shim, S.G. Lee, M. Lee, Biflavonoids isolated from Selaginella tamariscina and their anti-inflammatory activities via ERK 1/2 signaling, Molecules 23 (2018) 926, https://doi.org/10.3390/molecules23040926.
[70] B.Y.G. Mountessou, J. Tchamgoue, J.P. Dzoyem, R.T. Tchuenguem, F. Surup, M.I. Choudhary, S.F. Kouam, Two xanthones and two rotameric (3⟶ 8) biflavonoids from the Cameroonian medicinal plant Allanblackia floribunda Oliv. (Guttiferae), Tetrahedron Lett. 59 (2018) 4545–4550, https://doi.org/10.1016/j.tetlet.2018.11.035.
[71] J.W. Shou, R.R. Zhang, H.Y. Wu, X. Xia, H. Nie, R.W. Jiang, P.C. Shaw, Isolation of novel biflavonoids from Cardiocrinum giganteum seeds and characterization of their antitussive activities, J. Ethnopharmacol. 222 (2018) 171–176, https://doi.org/10.1016/j.jep.2018.05.003.
[72] M.M. Ndoile, F.R. Van Heerden, Antimalarial biflavonoids from the roots of Ochna serrulata (Hochst.) Walp, Int. Res. J. Pure Appl. Chem. 16 (2018) 1–9, https://doi.org/10.9734/IRJPAC/2018/42440.
[73] A. Al Groshi, H.A. Jasim, A.R. Evans, F.M. Ismail, N.M. Dempster, L. Nahar, S.D. Sarker, Growth inhibitory activity of biflavonoids and diterpenoids from the leaves of the Libyan Juniperus phoenicea against human cancer cells, Phytother. Res. 33 (2019) 2075–2082, https://doi.org/10.1002/ptr.6397.
[74] H. Wagner, L. Farkas, Synthesis of flavonoids, The Flavonoids, Springer, Boston-MA, 1975. https://doi.org/10.1007/978-1-4899-2909-9_4.
[75] D. Muller, J.P. Fleury, A new strategy for the synthesis of biflavonoids via arylboronic acids, Tetrahedron Lett. 32 (1991) 2229–2232, https://doi.org/10.1016/S0040-4039(00)79688-2.
[76] S.M. Ali, M. Ilyas, Biomimetic approach to biflavonoids: Oxidative coupling of 2'-hydroxychalcones with iodine in alkaline methanol, J. Org. Chem. 51 (1986) 5415–5417, https://doi.org/10.1021/jo00376a069.

[77] Y.M. Lin, M.T. Flavin, C.S. Cassidy, A. Mar, F.C. Chen, Biflavonoids as novel antituberculosis agents, Bioorg. Med. Chem. 11 (2001) 2101–2104, https://doi.org/10.1016/S0960-894X(01)00382-1.
[78] F.D. Riswanto, M.S. Rawa, V. Murugaiyah, N.H. Salin, E.P. Istyastono, M. Hariono, H.A. Wahab, Anti-cholinesterase activity of chalcone derivatives: synthesis, in vitro assay and molecular docking study, Med. Chem. 16 (2019) 1–11, https://doi.org/10.2174/1573406415666191206095032.
[79] S. Imran, M. Taha, N.H. Ismail, S.M. Kashif, F. Rahim, W. Jamil, H. Wahab, Synthesis of novel flavone hydrazones: In-vitro evaluation of α-glucosidase inhibition, QSAR analysis and docking studies, Eur. J. Med. Chem. 105 (2015) 156–170, https://doi.org/10.1016/j.ejmech.2015.10.017.
[80] S.S. Kim, V.A. Vo, H. Park, Synthesis of Ochnaflavone and Its Inhibitory Activity on PGE 2 Production, Bull. Korean Chem. Soc. 35 (2014) 3219–3223, https://doi.org/10.5012/bkcs.2014.35.11.3219.
[81] G. Sagrera, G. Seoane, Total Synthesis of 3′, 3‴-Binaringenin and Related Biflavonoids, Synthesis 2010 (2010) 2776–2786, https://doi.org/10.1055/s-0030-1258140.
[82] R.K. Nadirov, K.S. Nadirov, A.M. Esimova, Z.K. Nadirova, Electrochemical synthesis of amino derivatives of biflavonoids, Chem. Nat. Compd. 50 (2014) 735–736, https://doi.org/10.1007/s10600-014-1067-9.
[83] T.H. Sum, T.J. Sum, S. Collins, W.R. Galloway, D.G. Twigg, F. Hollfelder, D.R. Spring, Divergent synthesis of biflavonoids yields novel inhibitors of the aggregation of amyloid β (1–42), Org. Biomol. Chem. 15 (2017) 4554–4570, https://doi.org/10.1039/C7OB00804J.
[84] T.J. Sum, T.H. Sum, W.R. Galloway, D.G. Twigg, J.J. Ciardiello, D.R. Spring, Synthesis of structurally diverse biflavonoids, Tetrahedron 74 (2018) 5089–5101, https://doi.org/10.1016/j.tet.2018.05.003.
[85] M. Soto, R.G. Soengas, A.M. Silva, V. Gotor-Fernández, H. Rodríguez-Solla, Temperature-controlled stereodivergent synthesis of 2, 2′-biflavanones promoted by samarium diiodide, Chem. Eur. J. 25 (2019) 13104–13108, https://doi.org/10.1002/chem.201902927.
[86] K. Xu, C. Yang, Y. Xu, D. Li, S. Bao, Z. Zou, X. Yu, Selective geranylation of biflavonoids by Aspergillus terreus aromatic prenyltransferase (AtaPT), Org. Biomol. Chem. 18 (2020) 28–31, https://doi.org/10.1039/C9OB02296A.
[87] K. Anand, J. Ziebuhr, P. Wadhwani, J.R. Mesters, R. Hilgenfeld, Coronavirus main proteinase (3CLpro) structure: basis for design of anti-SARS drugs, Science 300 (2003) 1763–1767, https://doi.org/10.1126/science.1085658.
[88] X. Tian, G. Lu, F. Gao, H. Peng, Y. Feng, G. Ma, G.F. Gao, Structure and cleavage specificity of the chymotrypsin-like serine protease (3CLSP/nsp4) of porcine reproductive and respiratory syndrome virus (PRRSV), J. Mol. Biol. 392 (2009) 977–993, https://doi.org/10.1016/j.jmb.2009.07.062.
[89] L. Kiemer, O. Lund, S. Brunak, N. Blom, Coronavirus 3CL pro proteinase cleavage sites: Possible relevance to SARS virus pathology, BMC Bioinf. 5 (2004) 72, https://doi.org/10.1186/1471-2105-5-72.
[90] V. Thiel, K.A. Ivanov, A. Putics, T. Hertzig, B. Schelle, S. Bayer, A.E. Gorbalenya, Mechanisms and enzymes involved in SARS coronavirus genome expression, J. Gen. Virol. 84 (2003) 2305–2315, https://doi.org/10.1099/vir.0.19424-0.
[91] M.A. Alamri, M. Tahir Ul Qamar, M.U. Mirza, R. Bhadane, S.M. Alqahtani, I. Muneer, O.M. Salo-Ahen, Pharmacoinformatics and molecular dynamics simulation studies reveal potential covalent and FDA-approved inhibitors of SARS-CoV-2 main protease 3CLpro, J. Biomol. Struct. Dyn. (2020) 1–13, https://doi.org/10.1080/07391102.2020.1782768.
[92] A.K. Ghosh, M. Brindisi, D. Shahabi, M.E. Chapman, A.D. Mesecar, Drug development and medicinal chemistry efforts toward SARS-coronavirus and Covid-19 therapeutics, ChemMedChem (2020), https://doi.org/10.1002/cmdc.202000223 [Epub ahead of print].
[93] Mesecar AD. A taxonomically-driven approach to development of potent, broad-spectrum inhibitors of coronavirus main protease including SARS-CoV-2 (COVID-19), http://www.rcsb.org/structure/6W63; 2020 (accessed 24 October 2020).
[94] M. Stoermer, Homology models of coronavirus 2019-nCoV 3CLpro protease, ChemRxiv (2020).
[95] Z. Jin, X. Du, Y. Xu, Y. Deng, M. Liu, Y. Zhao, Y. Duan, Structure of M pro from SARS-CoV-2 and discovery of its inhibitors, Nature 582 (2020) 289–293, https://doi.org/10.1038/s41586-020-2223-y.
[96] L. Zhang, D. Lin, X. Sun, U. Curth, C. Drosten, L. Sauerhering, R. Hilgenfeld, Crystal structure of SARS-CoV-2 main protease provides a basis for design of improved α-ketoamide inhibitors, Science 368 (2020) 409–412, https://doi.org/10.1126/science.abb3405.
[97] H. Yang, M. Yang, Y. Ding, Y. Liu, Z. Lou, Z. Zhou, G.F. Gao, The crystal structures of severe acute respiratory syndrome virus main protease and its complex with an inhibitor, Proc. Natl. Acad. Sci. 100 (2003) 13190–13195, https://doi.org/10.1073/pnas.1835675100.
[98] F. Wang, C. Chen, W. Tan, K. Yang, H. Yang, Structure of main protease from human coronavirus NL63: insights for wide spectrum anti-coronavirus drug design, Sci. Rep. 6 (2016) 22677, https://doi.org/10.1038/srep22677.
[99] A. Acharya, R. Agarwal, M. Baker, J. Baudry, D. Bhowmik, S. Boehm, O. Demerdash, Supercomputer-based ensemble docking drug discovery pipeline with application to Covid-19, ChemRxiv (2020). Preprint. 10.26434/chemrxiv.12725465.v1.
[100] H.X. Su, S. Yao, W.F. Zhao, M.J. Li, L.K. Zhang, Y. Ye, Y.C. Xu, Identification of a novel inhibitor of SARS-CoV-2 3CLpro, Acta Pharmacol. Sin. 41 (2020) 1167–1177, https://doi.org/10.1038/s41401-020-0483-6.
[101] C. Ma, M.D. Sacco, B. Hurst, J.A. Townsend, Y. Hu, T. Szeto, J. Wang, Boceprevir, GC-376, and calpain inhibitors II, XII inhibit SARS-CoV-2 viral replication by targeting the viral main protease, Cell Res. 30 (2020) 678–692, https://doi.org/10.1038/s41422-020-0356-z.
[102] Mesecar AD. A taxonomically-driven approach to development of potent, broad-spectrum inhibitors of coronavirus main protease including SARS-CoV-2 (COVID-19), http://www.rcsb.org/structure/6W63; 2020 (accessed 24 October 2020).
[103] Z. Jin, Y. Zhao, Y. Sun, B. Zhang, H. Wang, Y. Wu, Y. Duan, Structural basis for the inhibition of SARS-CoV-2 main protease by antineoplastic drug carmofur, Nat. Struct. Mol. Biol. 27 (2020) 529–532, https://doi.org/10.1038/s41594-020-0440-6.
[104] Fearon, D., Owen, C.D., Douangamath, A., Lukacik, P., Powell, A.J., Strain-Damerell, C.M., & von Delft, F., PanDDA analysis group deposition SARS-CoV-2 main protease fragment screen, http://www.rcsb.org/structure/5RHF; 2020 (accessed 24 October 2020).
[105] Kneller DW, Phillips G, O'Neill HM, Jedrzejczak R, Stols L, Langan P, Kovalevsky A. Structural plasticity of SARS-CoV-2 3CL Mproactive site cavity revealed by room temperature X-ray crystallographyl http://www.rcsb.org/structure/6WQF; 2020 (accessed 24 October 2020).
[106] Kneller DW, Phillips G, O'Neill HM, Tan K, Joachimiak A, Coates L, Kovalevsky A, Room temperature X-ray crystallography reveals catalytic cysteine in the SARS-CoV-2 3CL Mpro is highly reactive: Insights for enzyme mechanism and drug design, http://www.rcsb.org/structure/6XB1; 2020 (accessed 24 October 2020).
[107] Wang H, He S, Deng W, Zhang Y, Li G, Sun J, Zhao W, Shang L. Comprehensive Insights into the Catalytic Mechanism of Middle East Respiratory Syndrome 3C-Like Protease and Severe Acute Respiratory Syndrome 3C-Like Protease, http://www.rcsb.org/structure/6LO0; 2020 (accessed 24 October 2020).
[108] Tan K, Maltseva NI, Welk LF, Jedrzejczak RP, Joachimiak A, The crystal structure of 3CL MainPro of SARS-CoV-2 with de-oxidized C145, http://www.rcsb.org/structure/7JFQ; 2020 (accessed 24 October 2020).
[109] Tan K, Maltseva NI, Welk LF, Jedrzejczak RP, Coates L, Kovalevskyi AY, Joachimiak, A. The crystal structure of 3CL MainPro of SARS-CoV-2 with oxidized Cys145 (Sulfenic acid cysteine), http://www.rcsb.org/structure/6XKF; 2020 (accessed 24 October 2020)
[110] Tan K, Maltseva NI, Welk LF, Jedrzejczak RP, Coates L, Kovalevsky A, Joachimiak A. The 1.28a crystal structure of 3cl mainpro of sars-cov-2 with oxidized c145 (sulfinic acid cysteine), http://www.rcsb.org/structure/6XKH; 2020 (accessed 24 October 2020)
[111] Tan K, Maltseva NI, Welk LF, Jedrzejczak RP, Joachimiak A. The crystal structure of 3CL MainPro of SARS-CoV-2 with C145S mutation, http://www.rcsb.org/structure/6XOA; 2020 (accessed 24 October 2020).
[112] Kneller DW, Phillips G, Weiss KL, Pant S, Zhang Q, O'Neill H. Kovalevsky A, Protonation states in SARS-CoV-2 main protease mapped by neutron crystallography http://www.rcsb.org/structure/7JUN; 2020 (accessed 24 October 2020).
[113] de Oliveira RR, Nascimento AFZ, Zeri ACM, Trivella DBB, SARS-CoV-2 3CL protease crystallized under reducing conditions, https://www.rcsb.org/structure/7JR3; 2020 (accessed 24 October 2020).
[114] Nascimento AFZ, de Oliveira RR, Zeri ACM, Trivella DBB. SARS-CoV-2 3CL protease with alternative conformation of the active site promoted by methylene-bridged cysteine and lysine residues, http://www.rcsb.org/structure/7JR4; 2020 (accessed 24 October 2020).
[115] Kneller DW, Phillips G, O'Neill HM, Tan K, Joachimiak A, Coates L, Kovalevsky, A. Room temperature X-ray crystallography reveals oxidation and reactivity of cysteine residues in SARS-CoV-2 3CL Mpro: Insights for enzyme mechanism and drug design, http://www.rcsb.org/structure/6XHU; 2020 (accessed 24 October 2020).
[116] Kneller DW, Galanie S, Phillips G, O'Neill HM, Coates L, Kovalevsky A. Extreme malleability of the SARS-CoV-2 3CL Mpro active site cavity facilitates binding of clinical antivirals: Prospects for repurposing existing drugs and ramifications for inhibitor design, http://www.rcsb.org/structure/6XQT; 2020 (accessed 24 October 2020).
[117] Rathnayake AD, Zheng J, Kim Y, Perera KD, Mackin S, Meyerholz DK, Kashipathy MM, Chang KO, 3C-like protease inhibitors block coronavirus replication in vitro and improve survival in MERS-CoV-infected mice, http://www.rcsb.org/structure/6W2A; 2020 (accessed 24 October 2020).
[118] Vuong W, Khan MB, Fischer C, Arutyunova E, Lamer T, Shields J, McKay RT, Lemieux MJ, Feline coronavirus drug inhibits the main protease of SARS-CoV-2 and blocks virus replication, http://www.rcsb.org/structure/6WTK; 2020 (accessed 24 October 2020).
[119] Ma C, Sacco M, Chen Y, Wang J. Crystal structure of the SARS-CoV-2 (COVID-19) main protease in complex with inhibitor UAW247, http://www.rcsb.org/structure/6XBH; 2020 (accessed 24 October 2020).
[120] Ma C, Sacco M, Chen Y, Wang J. Crystal structure of the SARS-CoV-2 (COVID-19) main protease in complex with inhibitor, http://www.rcsb.org/structure/6XBG; 2020 (accessed 24 October 2020).
[121] Sacco M, Chen Y, Ma C. Crystal structure of the SARS-CoV-2 (COVID-19) main protease in complex with UAW243, http://www.rcsb.org/structure/6XFN; 2020 (accessed 24 October 2020).
[122] Tan K, Maltseva NI, Welk LF, Jedrzejczak RP, Joachimiak A. The crystal structure of SARS-CoV-2 Main Protease in complex with masitinib, http://www.rcsb.org/structure/7JU7; 2020 (accessed 24 October 2020).
[123] Zhu L, Hilgenfeld R. Crystal structures of SARS-Cov main protease complexed with a series of unsaturated esters, http://www.rcsb.org/structure/3SZN; 2020 (accessed 24 October 2020).
[124] Zhu L, George S, Schmidt MF, Al-Gharabli SI, Rademann J, Hilgenfeld R. Peptide aldehyde inhibitors challenge the substrate specificity of the SARS-coronavirus main protease, http://www.rcsb.org/structure/3SNE; 2020 (accessed 24 October 2020).

[125] Ma C, Sacco M, Chen Y, Wang J, Crystal structure of the SARS-CoV-2 (COVID-19) main protease in complex with inhibitor UAW248, http://www.rcsb.org/structure/6XBI; 2020 (accessed 24 October 2020).
[126] Hoffman RL, Kania RS, Brothers MA, Davies JF, Ferre RA, Gajiwala KS, He M, Taggart B. The Discovery of Ketone-Based Covalent Inhibitors of Coronavirus 3CL Proteases for the Potential Therapeutic Treatment of COVID-19, http://www.rcsb.org/structure/6XHO; 2020 (accessed 24 October 2020).
[127] Sacco M, Chen Y, Ma C. Crystal structure of the SARS-CoV-2 (COVID-19) main protease in complex with UAW241, http://www.rcsb.org/structure/6XA4; 2020 (accessed 24 October 2020).
[128] Zhang L, Lin D, Sun, X, Curth U, Drosten C, Sauerhering L, Becker S, Hilgenfeld R. Crystal structure of SARS-CoV-2 main protease provides a basis for design of improved alpha-ketoamide inhibitors, http://www.rcsb.org/structure/6Y2E; 2020 (accessed 24 October 2020).
[129] Hattori SI, Higashi-Kuwata N, Hayashi H, Allu RS, Das D, Takamune N, Kishimoto N, Mitsuya H. A SARS-CoV-2's Main Protease-targeting Small-Compound GRL-2420 Completely Blocks the Infectivity and Cytopathicity of SARS-CoV-2, http://www.rcsb.org/structure/7JKV; 2020 (accessed 24 October 2020).
[130] Schmidt M, Malla, T. SARS cov-2 main protease 3clpro, room temperature, damage free xfel monoclinic structure, http://www.rcsb.org/structure/7JVZ; 2020 (accessed 24 October 2020).
[131] Littler DR, Gully BS, Colson RN, Rossjohn, J. Crystal Structure of the SARS-CoV-2 Non-structural Protein 9, Nsp9, http://www.rcsb.org/structure/6W9Q; 2020 (accessed 24 October 2020).
[132] Fu LF. Crystal structure of the 2019-nCoV main protease complexed with GC376, http://www.rcsb.org/structure/7BRR; 2020 (accessed 24 October 2020).
[133] Fu LF. Crystal structure of the 2019-nCoV main protease, http://www.rcsb.org/structure/7BRO; 2020 (accessed 24 October 2020).
[134] Fu LF. Crystal structure of the 2019-nCoV main protease complexed with Boceprevir, http://www.rcsb.org/structure/7BRP; 2020 (accessed 24 October 2020).
[135] Zhou XL, Zhong FL, Lin C, Hu XH, Zhou H, Wang QS, Li J, Zhang, J. The crystal structure of COVID-19 main protease in the apo state, http://www.rcsb.org/structure/7C2Q; 2020 (accessed 24 October 2020).
[136] Kuo CJ, Shie JJ, Lin CH, Lin YL, Hsieh MC, Lee CC, Chang SY, Liang PH. Complex Structures and Cellular Activities of the Potent SARS-CoV-2 3CLpro Inhibitors Guiding Drug Discovery Against COVID-19, http://www.rcsb.org/structure/7C8T; 2020 (accessed 24 October 2020).
[137] Kneller DW, Coates L, Kovalevsky, A. Structure of the complex between the SARS-CoV-2 Main Protease and Leupeptin, http://www.rcsb.org/structure/6XCH; 2020 (accessed 24 October 2020).
[138] Ye G, Wang X, Tong X, Shi Y, Fu ZF, Peng G. Structural Basis for Inhibiting Porcine Epidemic Diarrhea Virus Replication with the 3C-Like Protease Inhibitor GC376, http://www.rcsb.org/structure/6L70; 2020 (accessed 24 October 2020).
[139] Zhang L, Lin D, Kusov Y, Nian Y, Ma Q, Wang J, von Brunn A, Hilgenfeld, R., Alpha-ketoamides as broad-spectrum inhibitors of coronavirus and enterovirus replication Structure-based design, synthesis, and activity assessment, http://www.rcsb.org/structure/6FV1; 2020 (accessed 24 October 2020).
[140] Qiao JX, Zeng R, Li YS, Wang YF, Lei J, Yang SY. Crystal structure of SARS-CoV-2 main protease in complex with MI-23, http://www.rcsb.org/structure/7D3I; 2020 (accessed 24 October 2020).
[141] Fu LF, Feng Y, Qi JX, Crystal structure of SARS-Cov-2 main protease with narlaprevir, http://www.rcsb.org/structure/7D1O; 2020 (accessed 24 October 2020).
[142] Qiao JX, Zeng R, Wang YF, Li YS, Yao R, Zhou YL, Chen P, Yang SY. Crystal structure of the SARS-CoV-2 main protease in complex with Telaprevir, http://www.rcsb.org/structure/7C7P; 2020 (accessed 24 October 2020).
[143] Qiao JX, Zeng R, Wang YF, Li YS, Yao R, Liu JM, Zhou YL, Yang SY. Crystal structure of the SARS-CoV-2 main protease in complex with Boceprevir (space group P212121), http://www.rcsb.org/structure/7COM; 2020 (accessed 24 October 2020).
[144] Oerlemans R, Wang W, Lunev S, Domling A, Groves MR. Crystal structure of SARS CoV2 main protease in complex with inhibitor Boceprevir, http://www.rcsb.org/structure/6ZRU; 2020 (accessed 24 October 2020).
[145] Oerlemans R, Wang W, Lunev S, Domling A. Groves, M.R., Crystal structure of SARS CoV2 main protease in complex with inhibitor Telaprevir, http://www.rcsb.org/structure/6ZRT; 2020 (accessed 24 October 2020).
[146] Mohan K, Ueda G, Kim AR, Jude KM, Fallas JA, Guo Y, Hafer M, Garcia KC. Topological control of cytokine receptor signaling induces differential effects in hematopoiesis, http://www.rcsb.org/structure/6MOK; 2020 (accessed 24 October 2020).
[147] Dai W, Zhang B, Jiang XM, Su H, Li J, Zhao Y, Xie X, Liu H. Structure-based design of antiviral drug candidates targeting the SARS-CoV-2 main protease, http://www.rcsb.org/structure/6LZE; 2020 (accessed 24 October 2020).
[148] Fu L, Feng Y. Crystal structure of the SARS-CoV-2 main protease complexed with Boceprevir, http://www.rcsb.org/structure/7C6S; 2020 (accessed 24 October 2020).
[149] Qiao JX, Zeng R, Liu XL, Nan JS, Wang YF, Li YS, Lei J, Yang SY. Crystal structure of the SARS-CoV-2 main protease in complex with INZ-1, http://www.rcsb.org/structure/7CX9; 2020 (accessed 24 October 2020).
[150] V.S. Gontijo, W.A. Judice, B. Codonho, I.O. Pereira, D.M. Assis, J.P. Januário, C. V. Junior, Leishmanicidal, antiproteolytic and antioxidant evaluation of natural biflavonoids isolated from Garcinia brasiliensis and their semisynthetic derivatives, Eur. J. Med. Chem. 58 (2012) 613–623, https://doi.org/10.1016/j.ejmech.2012.06.021.
[151] V.S. Gontijo, J.P. Januário, W.A. de Souza Júdice, A.A. Antunes, I.R. Cabral, D.M. Assis, M.H. dos Santos, Morelloflavone and its semisynthetic derivatives as potential novel inhibitors of cysteine and serine proteases, J Med Plants Res 9 (2015) 426–434, https://doi.org/10.5897/JMPR2014.5641.
[152] D.M. Assis, V.S. Gontijo, Pereira I de Oliveira, J.A.N. Santos, I. Camps, T.J. Nagem, A.C. Doriguetto, Inhibition of cysteine proteases by a natural biflavone: behavioral evaluation of fukugetin as papain and cruzain inhibitor, J. Enzyme Inhib. Med. Chem. 28 (2013) 661–670, https://doi.org/10.3109/14756366.2012.668539.
[153] N.F. Fazio, M.H. Russell, S.M. Flinders, C.J. Gardner, J.B. Webster, M.D. Hansen, A natural product biflavonoid scaffold with anti-tryptase activity, Naunyn-Schmiedeberg's Arch. Pharmacol. (2020) 1–9, https://doi.org/10.1007/s00210-020-01959-2.
[154] C.W. Lee, H.J. Choi, H.S. Kim, D.H. Kim, I.S. Chang, H.T. Moon, E.R. Woo, Biflavonoids isolated from Selaginella tamariscina regulate the expression of matrix metalloproteinase in human skin fibroblasts, Bioorg. Med. Chem. 16 (2008) 732–738, https://doi.org/10.1016/j.bmc.2007.10.036.
[155] B.K. Yap, C.Y. Lee, S.B. Choi, E.E. Kamarulzaman, M. Hariono, H.A. Wahab, In silico identification of novel inhibitors, Ref Module Life Sci 3 (2019) 761–779, https://doi.org/10.1016/B978-0-12-809633-8.20158-1.
[156] S.N. Sulaiman, M. Hariono, H.M. Salleh, S.L. Chong, L.S. Yee, A. Zahari, K. Awang, Chemical constituents From Endiandra kingiana (Lauraceae) as potential inhibitors for dengue type 2 NS2B/NS3 serine protease and its molecular docking, Nat. Prod. Commun. 14 (2019). https://doi.org/10.1177%2F1934578X19861014.
[157] A. El Sahili, J. Lescar, Dengue virus non-structural protein 5, Viruses 9 (2017) 91, https://doi.org/10.3390/v9040091.
[158] A.R. Sahin, A. Erdogan, P.M. Agaoglu, Y. Dineri, A.Y. Cakirci, M.E. Senel, A.M. Tasdogan, 2019 novel coronavirus (COVID-19) outbreak: A review of the current literature, EJMO 4 (2020) 1–7, https://doi.org/10.14744/ejmo.2020.12220.
[159] L. Di, Strategic approaches to optimizing peptide ADME properties, AAPS J. 17 (2015) 134–143, https://doi.org/10.1208/s12248-014-9687-3.
[160] J. Swaminathan, C. Ehrhardt, Liposomal delivery of proteins and peptides, Expert Opin Drug Deliv 9 (2012) 1489–1503, https://doi.org/10.1517/17425247.2012.735658.
[161] M.R. Mozafari, Liposomes: an overview of manufacturing techniques, Cell. Mol. Biol. Lett. 10 (2005) 711.
[162] F.M. Tajabadi, M.R. Campitelli, R.J. Quinn, Scaffold Flatness: Reversing the Trend, Springer Sci Rev 1 (2013) 141–151, https://doi.org/10.1007/s40362-013-0014-7.
[163] A. Karshikoff, L. Nilsson, R. Ladenstein, Rigidity versus flexibility: the dilemma of understanding protein thermal stability, FEBS J. 2015 (282) (2015) 3899–3917.
[164] M. Hariono, S.H. Yuliani, E.P. Istyastono, F.D. Riswanto, C.F. Adhipandito, Matrix metalloproteinase 9 (MMP9) in wound healing of diabetic foot ulcer: Molecular target and structure-based drug design, Wound Med 22 (2018) 1–13, https://doi.org/10.1016/j.wndm.2018.05.003.
[165] E.P. Istyastono, N. Yuniarti, M. Hariono, S.H. Yuliani, F.D.O. Riswanto, Binary quantitative structure-activity relationship analysis in retrospective structure based virtual screening campaigns targeting estrogen receptor alpha, Asian J. Pharm. Clin. Res. 10 (2017) 206–211, https://doi.org/10.22159/ajpcr.2017.v10i12.20667.